

Chain-of-Evidence Multimodal Reasoning for Few-shot Temporal Action Localization

Mengshi Qi, *Member, IEEE*, Hongwei Ji, Wulian Yun, Xianlin Zhang, Huadong Ma, *Fellow, IEEE*

Abstract—Traditional temporal action localization (TAL) methods rely on large amounts of detailed annotated data, whereas few-shot TAL reduces this dependence by using only a few training samples to identify unseen action categories. However, existing few-shot TAL methods typically focus solely on video-level information, neglecting textual information, which can provide valuable semantic support for the action localization task. To address these issues, in this work, we propose a new few-shot temporal action localization method by Chain-of-Evidence multimodal reasoning to improve localization performance. Specifically, we design a novel few-shot learning framework to capture action commonalities and variations, which includes a semantic-aware text-visual alignment module designed to align the query and support videos at different levels. Meanwhile, to better express the temporal dependencies and causal relationships between actions at the textual level, we design a Chain-of-Evidence (CoE) reasoning method that progressively guides the Vision Language Model (VLM) and Large Language Model (LLM) to generate CoE text descriptions for videos. The generated texts can capture more variance of action than visual features. We conduct extensive experiments on the publicly available ActivityNet1.3, THUMOS14 and our newly collected *Human-related Anomaly Localization Dataset*. The experimental results demonstrate that our proposed method significantly outperforms existing methods in single-instance and multi-instance scenarios. Our source code and data are available at <https://github.com/MICLAB-BUPT/VAL-VLM>.

Index Terms—Few-shot Learning, Temporal Action Localization, Multimodal Reasoning

I. INTRODUCTION

WITH the rapid development of social media platforms, such as TikTok and Instagram, the number of short videos has increased tremendously, creating a significant challenge in effectively managing and utilizing large amounts of video resources. Consequently, the importance of video understanding has become more evident.

Specially, Temporal Action Localization (TAL) [1]–[7] as a crucial task in video understanding, aims to detect the start and end times of action instances in untrimmed videos. However, existing fully-supervised TAL methods rely on large amounts of precise temporal annotations for training, requiring substantial data for each category, which is both time-consuming and costly. Furthermore, these methods can only identify action

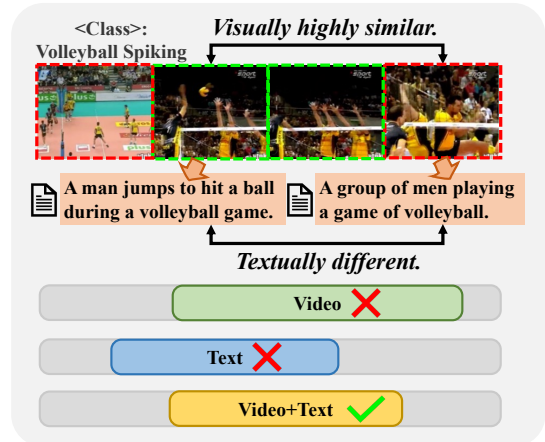


Fig. 1. Illustration of the assistance of multimodal information in few-shot TAL task. Most of existing methods that rely solely on visual information often misjudge when distinguishing between highly similar foreground (green dashed box) and background (red dashed box) snippets. The text provides more semantic details, helping the model achieve more precise predictions.

categories present in the training and lack the ability to predict unseen categories, limiting their practical application.

Nowadays, few-shot learning [8]–[12] has shown impressive performance in computer vision tasks, providing a novel solution to the above challenges. By mimicking the human ability to learn from limited labeled samples, models can quickly adapt to new tasks or categories. Few-shot learning can be roughly classified into two categories: meta-learning [9], [10] and transfer learning [12], [13]. Meta-learning enhances the model’s ability to quickly adapt to new tasks by training it on multiple tasks, while transfer learning reduces data requirements by transferring knowledge from existing tasks to new ones. Therefore, few-shot learning can be introduced into TAL tasks to enable the model to localize actions in unseen videos using limited data.

Current few-shot TAL methods [14]–[19] mainly rely on meta-learning, aligning query and support videos to capture commonalities and variations within the same action category. This enables the model to effectively apply learned knowledge to new classes. However, extracting variations and commonalities from a limited number of samples becomes challenging. In contrast, textual information explicitly describes the action’s semantic content and context, helping the model capture its commonalities and variations more effectively. Especially, text descriptions of a short video at various timestamps can bring larger differences than visual appearance. To be specific, recent advancements in pre-trained VLMs [20]–[22] offer a new perspective on this issue. VLMs provide additional prior knowledge by learning joint visual-textual representations from large-scale datasets, particularly in modeling person-

This work is partly supported by the Funds for the NSFC Project (Grant 62572072, U24B20176) and Beijing Natural Science Foundation (L243027). (Corresponding author: Mengshi Qi and Xianlin Zhang (email: qms@bupt.edu.cn))

M. Qi, H. Ji, W. Yun, X. Zhang and H. Ma are with State Key Laboratory of Networking and Switching Technology, Beijing University of Posts and Telecommunications, China.

object relationships. For example, the semantic information provided by the text generated by the VLMs effectively helps distinguish the athlete’s spike action from ordinary volleyball scenes. Relying solely on visual information, the model finds it challenging to differentiate between these two visually similar contents, which leads to difficulties in accurate localization as shown in Figure 1. Therefore, how to effectively integrate multimodal information including texts, images and videos into few-shot TAL tasks, leverage differences in textual representations to overcome the limitations of visual features, enhance the distinction between visually similar content, and improve the consistency between query and support videos remains a challenge.

Furthermore, a number of methods [23], [24] provide frame-level video descriptions while ignoring that the occurrence of actions is often accompanied by temporal dependencies and causal relationships. For example, after a player catches the basketball, the next likely action is to shoot. It is still difficult for the model to accurately identify such action sequences and their underlying connections. Therefore, generating text that effectively expresses these dependencies and causal relationships to guide few-shot TAL task, thereby enhancing the model’s understanding of dynamic relationships between actions will be promising.

To address the above-mentioned issues, we propose a novel few-shot TAL method, which utilizes textual semantic information to assist the model in capturing both commonalities and variations within the same class, thereby enhancing localization performance. First, we propose a Chain-of-Evidence (CoE) reasoning method, which hierarchically guides VLM and LLM to identify the temporal dependencies of actions and the causal relationships between actions, thereby generating structured CoE textual descriptions. Next, we employ a semantic-temporal pyramid encoder and the CLIP text encoder to extract video and text features across hierarchical levels from the query and support video, and their corresponding text. Subsequently, we design a semantic-aware text-visual alignment module to perform multi-level alignment between videos and texts, leveraging semantic information to capture both commonalities and variations in actions. Finally, the aligned features are fed into the prediction head to generate action proposals. In addition, we explore human-related anomalous events to expand the application scope of few-shot action localization and introduce the first human-related anomaly localization dataset.

Our contributions can be summarized as follows:

- We introduce a new few-shot learning method for the TAL task, which leverages hierarchical video features with textual semantic information to enhance the alignment of query and support.
- We design a novel Chain-of-Evidence reasoning method to generate textual descriptions to effectively and explicitly describe temporal dependencies and causal relationships between actions.
- We collect and annotate the first benchmark for human-related anomaly localization, which includes 12 types of anomalies, 1,159 videos and more than 2,543,000 frames in total.

- We achieve state-of-the-art performance on public benchmarks, attaining improvements of about 4% on the ActivityNet1.3 dataset and 12% on the THUMOS14 dataset under the multi-instance 5-shot scenario compared to the other state-of-the-art methods.

II. RELATED WORK

Temporal Action Localization (TAL). TAL [1]–[4], [7], [25]–[28] is an essential task in video understanding [29]–[42], which aims to locate the start and end times of actions in untrimmed videos. Prevailing fully-supervised methods can be categorized into *two-stage* and *one-stage* approaches. *Two-stage* methods first generate a set of candidate proposals, which are then classified and refined. This paradigm has evolved from early sliding-window strategies [1] towards boundary-aware networks [25], with subsequent efforts incorporating temporal structural modeling [2] and graph reasoning [26] to further improve proposal quality. In contrast, *one-stage* methods directly predict action boundaries and labels in a single pass to improve efficiency. This category spans from anchor-based approaches [5] to recent anchor-free Transformer architectures [4], [7], [27]. However, all the aforementioned methods rely on a large amount of accurate annotations, making them costly and difficult to generalize to unseen classes. Moreover, most of them focus on common daily and sports activities, neglecting critical applications like localizing human-related anomalies.

Few-shot Learning (FSL). FSL aims to enable models to adapt to new categories or tasks from limited training data. It can be roughly divided into two major categories: meta-learning [8], [10] and transfer-learning [12], [13]. Considering the similar data scarcity challenges in TAL, few-shot learning has been introduced to address these issues, primarily following the meta-learning paradigm. Early works [14] focused on aligning global representations of query and support videos. Subsequent research improved alignment quality by introducing multi-level feature correspondence [43], Query-Adaptive Transformers [16], or cross-correlation attention modules [19]. Concurrently, other studies explored richer context modeling. These approaches extend alignment to the spatial-temporal domain using Transformers [15], leverage bilateral attention for context awareness [18], or utilize Context Graph Convolutional Networks [44] to aggregate information. Although these methods have achieved significant progress in visual alignment and context modeling, they almost solely rely on cues derived from the visual modality. This reliance becomes a critical bottleneck in visually ambiguous scenarios and diminishes the accuracy of the localization. To overcome the limitations of visual-only alignment in prior works, we leverage textual semantic information to assist in the query-support alignment, which enhances the model’s performance when facing complex cases.

Large Language Models. The emergence of Large Language Models (LLMs) has a significant impact on Natural Language Processing, demonstrating a superior ability to generalize across unseen tasks via in-context learning. Representative works like the GPT series [45], [46] and open-source LLaMA variants [47], [48] exhibit remarkable performance across

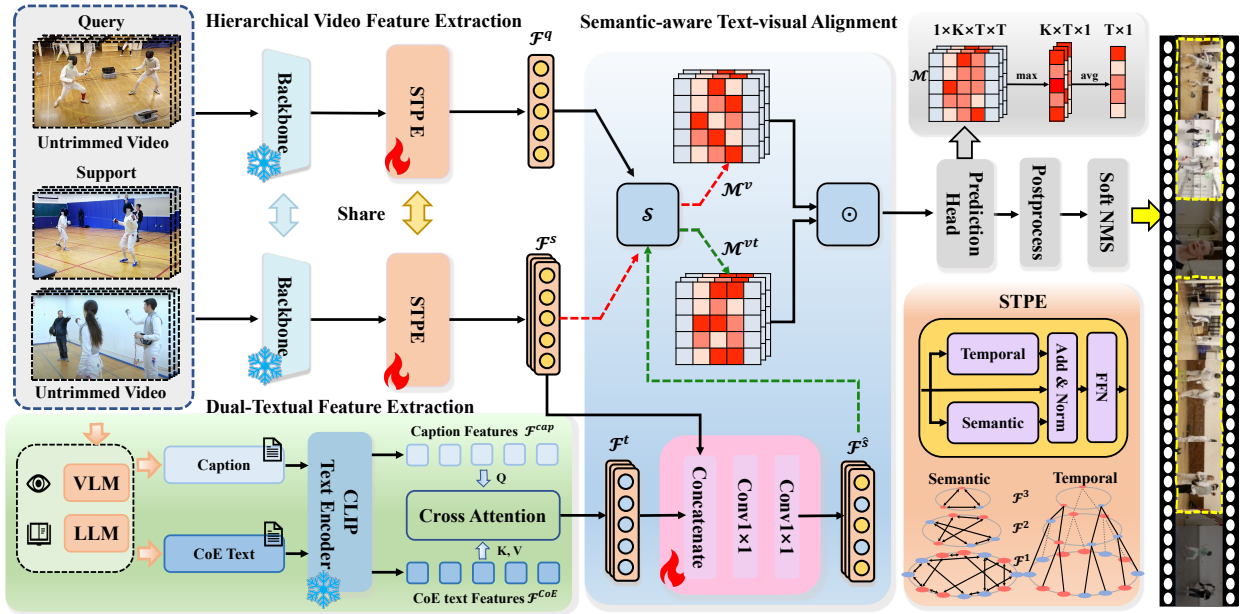


Fig. 2. Overall framework of our proposed method. We take three inputs: query video, support videos, and the corresponding support text. First, the query video and support videos are processed through a pre-trained backbone, followed by feature extraction by the semantic-temporal pyramid encoder (STPE). Next, the textual features of the support text are extracted using the CLIP Text Encoder. Then, the features from the captions and CoE text undergo cross-attention to obtain enhanced textual features. Subsequently, the query video features, support video features, and enhanced textual features are input into the semantic-aware text-visual alignment module. Finally, the aligned features are passed to the prediction head to generate action proposals.

domains. Building on this, researchers have extended LLMs to visual tasks. LLaVA [49], [50] aligns modalities via instruction tuning, while subsequent works like VideoChat [20] and InternVL [51] further advance temporal understanding and visual encoder scaling. Recently, DeepSeek-R1 [52] demonstrated that Chain-of-Thought (CoT) [53] significantly enhances reasoning by decomposing complex problems. The Chain-of-Thought (CoT) [53] paradigm empowers models to decompose complex problems into sequential reasoning steps. The reasoning capability elicited by CoT is crucial for Temporal Action Localization (TAL), particularly in identifying complex anomalous events, which are characterized by intrinsic logical and causal relationships. Conventional textual data, such as captions, are inadequate to express this structured logic. Therefore, we design a new Chain-of-Evidence (CoE) reasoning which is similar to the CoT to indirectly incorporate the reasoning capabilities of models like DeepSeek-R1 into the TAL task to improve the localization performance, especially by adding more logical analysis of evidence through causal reasoning.

III. PROPOSED METHOD

A. Overview

Problem Definition. For the few-shot TAL task, given a training set $D_{\text{train}} = \{(x, y) \mid x \in \mathcal{X}_{\text{train}}, y \in \mathcal{C}_{\text{train}}\}$ and a test set $D_{\text{test}} = \{(x, y) \mid x \in \mathcal{X}_{\text{test}}, y \in \mathcal{C}_{\text{test}}\}$. Specifically, x denotes the input video and $y = (c, t_s, t_e)$ represents labels, where c denotes the action category, t_s and t_e represent the start and end time of the action instance, respectively. Note that the labels of these two sets are disjoint, *i.e.*, $\mathcal{C}_{\text{train}} \cap \mathcal{C}_{\text{test}} = \emptyset$. Under the K -shot setting, each localization task comprises a query video v^q and K support videos $\{v_i^s\}_{i=1}^K$ with frame-level labels. Our objective is to train a model on D_{train} that

generalizes to D_{test} , enabling it to localize actions in the untrimmed query video by utilizing the annotated support videos.

Our proposed architecture is shown in Figure 2, which mainly consists of Hierarchical Video Feature Extraction, Dual-Textual Feature Extraction, and Semantic-Aware Text-Visual Alignment. Finally, the aligned multi-modal features are passed to the prediction head to perform action localization.

B. Hierarchical Video Feature Extraction

Given an untrimmed query video v^q and a set of untrimmed support videos $\{v_i^s\}_{i=1}^K$, where K denotes the number of support videos, we first extract features from all the videos. Specifically, we first follow [16], [44] to divide the video into non-overlapping snippets, and adopt a pre-trained backbone, *i.e.*, C3D [54], to extract snippet-level features. Then these features are rescaled to a fixed temporal dimension T using linear interpolation. These features are subsequently fed into our proposed Semantic-Temporal Pyramid Encoder to capture more robust features from temporal and semantic levels. Finally, we obtain the feature representation $\mathcal{F}^q \in \mathbb{R}^{1 \times T \times D}$ and $\mathcal{F}^s \in \mathbb{R}^{K \times T \times D}$ of the query video and support videos, where T denotes the number of snippets and D is the feature dimension.

Semantic-Temporal Pyramid Encoder. The visual feature primarily focuses on local motion information, neglecting the modeling of long-term temporal dependencies and semantic relationships. As a result, it fails to adequately capture the temporal sequence of actions and their intrinsic connection with the context. To address this, we propose a new semantic-temporal pyramid encoder (STPE) to enhance the modeling of both semantic features and long-temporal dependencies at

hierarchical levels, as shown in Figure 2. Our STPE mainly contains a temporal pyramid block and a semantic pyramid block. First, we follow [55] to establish a pyramid structure to obtain feature representations at different scales. Given a video feature $\mathcal{F}^1 = \{f_1^1, f_2^1, \dots, f_T^1\}$ generated by C3D, where f_t^1 , ($t = 1, 2, \dots, T$) denotes the snippet feature, we sequentially perform several snippet-level convolution operations along the temporal dimension of the video features \mathcal{F} , we can extract feature sequences at various scales, which can be expressed as follows:

$$\mathcal{F}^{k+1} = \{\Theta(f_1^k, f_2^k, f_3^k), \dots, \Theta(f_{T-2}^k, f_{T-1}^k, f_T^k)\}, \quad (1)$$

where Θ represents the convolution layer with a kernel size of 3 and a stride of 3, and $\mathcal{F}^{k+1} \in \mathbb{R}^{\lfloor \frac{T}{3^k} \rfloor \times D}$ ($k = 1, 2, \dots$) represents the features after k snippets-level convolution operations. Subsequently, we stack these feature sequences to form the pyramid structure, as illustrated in Figure 2. For each feature f_t^1 in \mathcal{F}^1 , we compute the temporal attention by considering its adjacent features $\{f_{t-1}^1, f_{t+1}^1\}$ in the same layer, as well as the feature $f_{\lfloor \frac{t+1}{3} \rfloor}^2 = \Theta(f_{t-1}^1, f_t^1, f_{t+1}^1)$ from the subsequent layer obtained through convolution using the Eq. (1). The same attention operation is also performed for other features in the same layer and the higher layers.

However, relying solely on long-term temporal modeling is insufficient for accurately localizing action boundaries, as it fails to capture the intrinsic contextual connections. Therefore, we propose the semantic pyramid block to explore the semantic relationships between snippets. For each feature f_t^k in \mathcal{F}^k , we only need to focus on the m most similar features within the same layer to perform a semantic attention operation. Specifically, we compute a pairwise cosine similarity matrix $S \in \mathbb{R}^{\lfloor \frac{T}{3^k} \rfloor \times \lfloor \frac{T}{3^k} \rfloor}$ ($k = 1, 2, \dots$) for all features within the layer. For each feature f_t^k , we select the m features with the highest similarity scores to form its dynamic semantic nodes $\mathcal{F}^{sim} \in \mathbb{R}^{m \times D} = \{f_a^k, f_b^k, \dots\}$. This approach not only helps reduce the computational burden but also enhances the discrimination among features. The learning process can be formulated as:

$$Attn(f_t^k) = softmax\left\{\frac{f_t^k W_Q}{\sqrt{D}} (\mathcal{F}^{sim} W_K)^T\right\} \cdot (\mathcal{F}^{sim} W_V), \quad (2)$$

where W_Q, W_K, W_V are learnable parameters and D is the feature dimension. The semantic pyramid block enhances the semantic connections across different snippet scales, consolidating commonalities and strengthening variations within the class. After processing through the two pyramids, a residual connection and a feed-forward neural network are applied. Finally, we obtain the query video features \mathcal{F}^q and support video features \mathcal{F}^s .

C. Dual-Textual Feature Extraction

For the video in the support set, we pre-generate the frame-level captions and CoE textual descriptions utilizing the VLM and LLM, as shown in Figure 3. More details about CoE textual descriptions generation please refer to Section IV-B. Subsequently, the above descriptions are processed through

CLIP Text Encoder [56] to extract the corresponding caption features $\mathcal{F}^{cap} \in \mathbb{R}^{1 \times K \times T \times D}$ and CoE text features $\mathcal{F}^{CoE} \in \mathbb{R}^{1 \times K \times T' \times D}$. Here, the dimension T' corresponds to the number of sentences in the generated CoE description of the video. To combine the temporal nature of the caption with the CoE text features, we apply cross-attention between the two to generate the final text feature $\mathcal{F}^t \in \mathbb{R}^{1 \times K \times T \times D}$ for assisting the TAL task, which can be formulated as:

$$\mathcal{F}^t = softmax\left\{\frac{\mathcal{F}^{cap} W_Q}{\sqrt{D}} (\mathcal{F}^{CoE} W_K)^T\right\} \cdot (\mathcal{F}^{CoE} W_V), \quad (3)$$

where W_Q, W_K, W_V are learnable parameters and D is the feature dimension. This approach enables us to effectively combine these two types of features while preserving the temporal sequence of the caption features and introducing greater coherence and comprehensiveness.

D. Semantic-Aware Text-Visual Alignment

After obtaining the video feature representations of the query and support, as well as the textual features, denoted as \mathcal{F}^q , \mathcal{F}^s , and \mathcal{F}^t . We design a new semantic-aware text-visual alignment module. Firstly we align the video features \mathcal{F}^q and \mathcal{F}^s of query and support, where we utilize cosine similarity to measure the degree of alignment between a query-support snippet pair, resulting in the video alignment map $\mathcal{M}^v \in \mathbb{R}^{1 \times K \times T \times T}$, formulated as follows:

$$\mathcal{M}^v = \mathcal{S}(\mathcal{F}^q, \mathcal{F}^s), \quad (4)$$

where \mathcal{S} denotes cosine similarity. However, solely relying on \mathcal{M}^v to align the query and support action snippets may result in inaccurate alignments, particularly when snippet pairs are irrelevant but share highly similar action backgrounds. Hence, we introduce textual information that can explicitly describe the action and background context, aiding in the capture of commonalities and variations.

Then, we align the support text features \mathcal{F}^t with the support video features \mathcal{F}^s to obtain video-text aligned features $\mathcal{F}^{\hat{s}} \in \mathbb{R}^{K \times T \times D}$ of the support video. We first concatenate the features from two modalities along the feature dimension and apply two 1x1 convolutions for alignment, which are formulated as:

$$\mathcal{F}^{\hat{s}} = \Theta(\sigma(\Theta(\mathcal{F}^t \oplus \mathcal{F}^s))), \quad (5)$$

where Θ denotes the convolution operation, σ represents the ReLU activation function, and \oplus means the concatenation along the feature dimension. In this way, we align the features from both modalities, enriching the support set and providing additional auxiliary information for the subsequent query and support video alignment. Subsequently, to align between the video features \mathcal{F}^q of query and video-text aligned features $\mathcal{F}^{\hat{s}}$ of the support, we calculate the video-text alignment map $\mathcal{M}^{vt} \in \mathbb{R}^{1 \times K \times T \times T}$ in the same manner of \mathcal{M}^v :

$$\mathcal{M}^{vt} = \mathcal{S}(\mathcal{F}^q, \mathcal{F}^{\hat{s}}). \quad (6)$$

Relying solely on the video alignment map \mathcal{M}^v to align the query and support can easily lead to the misalignment of visually similar foreground and background snippets. In

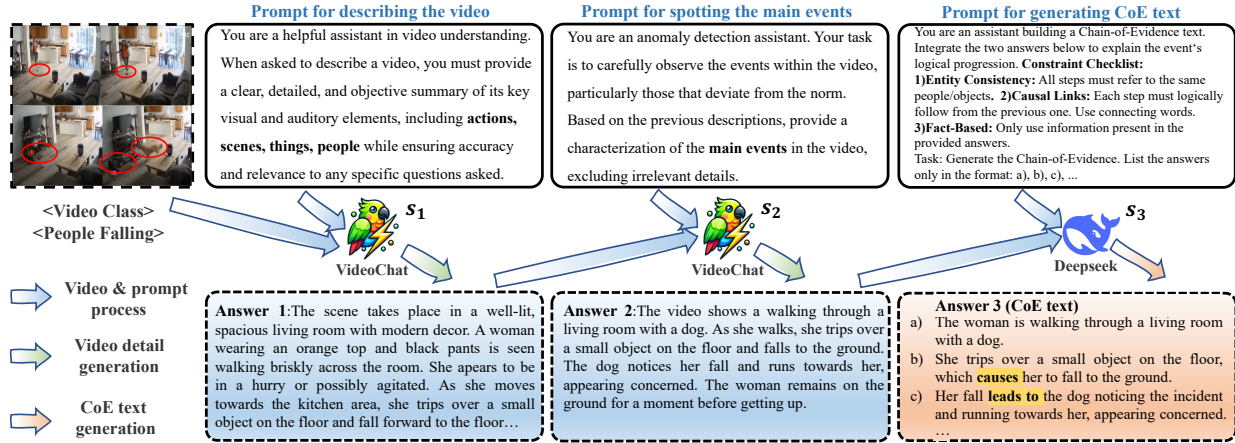


Fig. 3. An overview of CoE reasoning. We first prompt (\rightarrow) the VLM to generate details of the video and the process of the human action (or anomaly event) for the given video (\rightarrow). Next, we ask the LLM to generate CoE text based on the details and event sequence provided by the VLM (\rightarrow). The logical connectors in the CoE text (Answer 3) have been highlighted in yellow.

contrast, the video-text alignment map \mathcal{M}^{vt} leverages the clarity of textual semantics to reduce such occurrences. Therefore, we perform an element-wise multiplication of the two maps, using the video-text alignment map \mathcal{M}^{vt} to correct the erroneous regions in the video alignment map \mathcal{M}^v . Besides, the background snippets often vary significantly across different support samples, so we concentrate on aligning action commonalities within the foreground snippets by applying a background snippets masking operation on the alignment map. The entire process can be formulated as:

$$\mathcal{M} = \mathcal{M}^v \odot \mathcal{M}^{vt} \odot \mathcal{M}^m, \quad (7)$$

where $\mathcal{M} \in \mathbb{R}^{1 \times K \times T \times T}$, \odot is the element-wise multiplication and \mathcal{M}^m is the background snippets mask matrix. Finally, we utilize a prediction head to obtain the snippet-level predicted result denoted as $\hat{p} \in \mathbb{R}^{1 \times T}$.

E. Optimization and Inference

Loss function. To optimize our proposed model, we follow [57] to employ the cross-entropy loss, which consists of two snippet-level losses, *i.e.*, \mathcal{L}_{fg} and \mathcal{L}_{bg} . The total loss function \mathcal{L} can be defined as:

$$\mathcal{L} = \mathcal{L}_{fg} + \mathcal{L}_{bg}. \quad (8)$$

For better classifying the foreground snippet when there are only a few foreground or background snippets present in a query video during the training, we introduce k_{fg} and k_{bg} to deal with the unbalanced issue as follows:

$$k_{fg} = \min\left(t, \frac{t}{t_{fg} + \varepsilon}\right), \quad (9)$$

$$k_{bg} = \min\left(t, \frac{t}{t_{bg} + \varepsilon}\right),$$

where t , t_{fg} and t_{bg} are the number of total snippets, foreground snippets, and background snippets, respectively. Additionally, minimum operation and ε are used to avoid situations with excessively large k and where the divisor is

zero. With the adjustment ratios k_{fg} and k_{bg} , the two snippet-level loss functions can be described as:

$$\mathcal{L}_{fg} = -k_{fg} \sum_{i=1}^T y(i) \log[\hat{p}(i)], \quad (10)$$

$$\mathcal{L}_{bg} = -k_{bg} \sum_{i=1}^T [1 - y(i)] \log[1 - \hat{p}(i)],$$

where y is the query ground truth mask and $\hat{p} \in \mathbb{R}^{1 \times T}$ represents the snippet-level prediction.

Inference. During the reference, we randomly select a novel class from C_{test} , which has never been seen before. For each selected class, we choose $1+k$ videos as query and support to form a k -shot localization task, along with the action snippet annotations of the support. For each query video, we generate the foreground probability of each snippet by applying the frozen model. Subsequently, we select the consecutive snippets as proposals where the foreground probability exceeds a predefined threshold. Additionally, we filter out the too-short proposals and calculate the average probability as confidence for the remaining proposals. We then refine the proposals using soft non-maximum suppression (SNMS) [58] with a threshold of 0.7.

IV. THE HAL BENCHMARK

To extend the application of temporal action localization to the more practical domains such as human-related anomaly detection, we construct a new Human-related Anomaly Localization (HAL) benchmark. The core feature of HAL is the Chain-of-Evidence (CoE) textual descriptions that we newly generated. Compared to the textual information used in prior works [23], [59], [60], this new format is richer in logic and more clearly structured. To efficiently generate the CoE texts, we design an automated CoE reasoning pipeline that guides the VLM and LLM to perform reasoning about the evidence of the causal inference in the video content. The goal is to leverage this causality-infused text to indirectly imbue the localization task with the reasoning capabilities of LLMs, which allows the model to achieve a more precise understanding and localization of complex anomalous events.

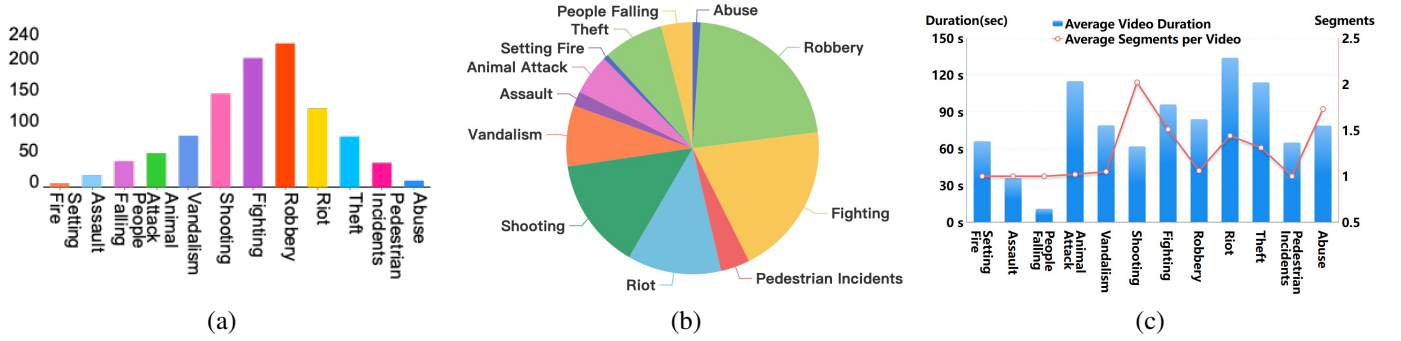


Fig. 4. Statistical overview of the proposed Human-related Anomaly Localization (HAL) dataset. (a) Distribution of the number of videos for each of the 12 anomaly categories. (b) Proportions of each anomaly category in the dataset. (c) Average duration (in seconds) and the number of distinct anomaly segments per video for each category.

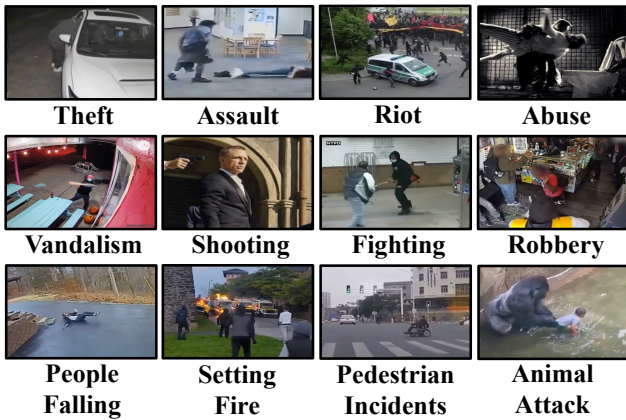


Fig. 5. Illustration of 12 anomaly types in our collected HAL dataset.

A. Data Source

Current TAL datasets [61]–[63] primarily focus on identifying sports and daily activities. However, the task of localizing human anomalous activities is more significant in practical applications, which is of vital importance to the safety of people’s lives and property. Hence, we manually select anomalous videos related to human activities from three large-scale anomaly datasets, namely MSAD [64], XD-Violence [65], and CUVA [66], and construct the Human-related Anomaly Localization dataset. This dataset contains 12 types of human-related anomalous behaviors, such as fighting, people falling, and robbery, as shown in Figure 4 and 5. In total, there are 1,072 videos with a cumulative duration of 26.3 hours, comprising over 2,543,000 frames. Each video is accompanied by frame-level annotations of anomaly intervals, along with corresponding frame captions and CoE text.

B. Chain-of-Evidence Reasoning Pipeline

To generate texts that adequately represent the temporal dependencies and causal relationships between actions, we propose a new CoE reasoning method, as shown in Figure 3. Our method employs a hierarchical, stage-wise process to guide the VLM and LLM in progressively generating structured, CoE textual descriptions, with each stage refining the prior output to enhance action understanding.

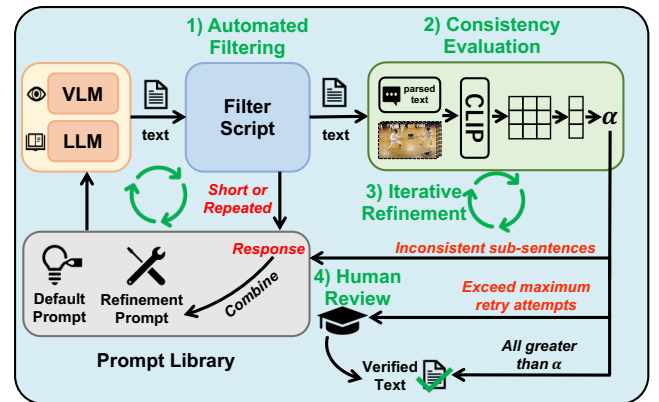


Fig. 6. The validation pipeline for the generated text.

Specifically, the reasoning process is explicitly decomposed into three progressive stages. Each stage $s_t = (p_t, x_{t-1}, o_t)$ consists of the prompt p_t , the input x_{t-1} from previous steps and the corresponding textual output o_t . First, for each video x , we utilize the VLM (*i.e.*, VideoChat [20]) to generate the detailed video descriptions denoted as $s_1 = (p_1, x_0, o_1)$. Although these descriptions provide detailed depictions of the entire video, they also introduce substantial noisy information. Therefore, we further guide the VLM to filter out such redundant information, enabling it to focus on the most critical actions or anomalous snippets. This process can be denoted as $s_2 = (p_2, x_1, o_2)$. Building upon this, we further guide the reasoning LLM, such as DeepSeek-R1 [52], to perform in-depth logical analysis and reasoning on the generated video-level descriptions o_1 and o_2 , enabling the identification of action sequences and underlying causal relationships. The subsequent reasoning process can be represented as $s_3 = (p_3, x_2, o_3)$, where $x_2 = \{o_1, o_2\}$, $o_3 = \{c_1, c_2, \dots\}$, c_i can be a sub action e from $\{o_1, o_2\}$ or a causal link $e_i \rightarrow e_{i+1}$. Taking Figure 3 as an example, the first element c_1 in o_3 describes a standalone action (e_1): “The woman is walking through a living room with a dog.” The following elements then capture causal links $e_i \rightarrow e_{i+1}$, explicitly stating that “She trips over a small object... (e_1) which **causes** her to fall (e_2)” and “Her fall (e_2) **leads to** the dog noticing the incident... (e_3)” thereby constructing chains of evidence. To ensure the coherence and logical integrity of the generated chain, the prompt p_3 is

specifically engineered to instruct the LLM to maintain consistency with the entities, scenes, and temporal flow established in the previous stages. By explicitly tasking the model with identifying and connecting key events, the prompt activates the inherent reasoning capabilities to construct a coherent narrative, where each step logically follows from the last. This prevents disconnected or contradictory statements and ensures a chain-like structure in the final output o_3 . Through this multi-stage generation process, the resulting text progressively presents a structured CoE description. Finally, we generate approximately 7,000, 87,000, and 2,400 CoE texts for the HAL, ActivityNet1.3 [61] and THUMOS14 [62], respectively.

C. Generated Texts Verification Pipeline

To ensure the quality of our generated CoE texts, we designed a validation pipeline for the output of each stage during Chain of Evidence reasoning. **1) Automated Filtering:** We first use scripts to filter out entries with formatting errors or invalid content in the text, such as overly short or repetitive responses. This step quickly removes many low-quality outputs. **2) Consistency Evaluation:** To quantify semantic alignment, we employ a CLIP-based evaluation method. We first parse it into sub-sentences based on punctuation or logical connectors and sample the video at 1 fps. Subsequently, we utilize the CLIP encoders to extract the textual and visual features. Then we compute a cosine similarity matrix $S \in \mathbb{R}^{N_{sent} \times N_{frame}}$ for the sub-sentence and frame features, where N_{sent} and N_{frame} represent the number of sub-sentences and frames, respectively. For each sub-sentence, a matching score is derived by averaging its Top-3 highest similarities. Sub-sentences falling below a predefined threshold α are identified as inconsistent and returned for refinement. **3) Iterative Refinement:** We implement a feedback-driven mechanism where inconsistent sub-sentences are injected into a refined prompt alongside the context to guide the language model to specifically revise the inconsistent part, after which the output is re-evaluated through step 2. **4) Human Review:** Cases failing validation after fixed retries (*e.g.*, 5) are routed to human review. To ensure reliability, the threshold α is pre-calibrated via human cross-validation on a seed dataset. Through this iterative self-refined pipeline, we significantly alleviate the hallucinations and ensure the quality of the CoE text in our benchmark. The details of the algorithm can be referred to in the appendix.

V. EXPERIMENTS

A. Datasets and Evaluation Metrics

ActivityNet1.3 Dataset [61] covers 200 actions, containing 19,994 untrimmed videos. Following [67], we split the 200 classes into three subsets without any overlap for training (80%), validation (10%) and testing (10%), respectively. For the single-instance scenario, we adopt videos that contain one action snippet. For multi-instance scenarios, we utilize the original videos after filtering out those that contain more than one class category. Hence, we remove the videos with invalid links, leaving approximately 16,800 videos in the final.

THUMOS14 Dataset [62] covers 20 action categories, with 200 validation videos and 213 test videos. We reconstruct the

dataset division for the meta-learning strategy as in [14]. The ratio of the number of training, validation, and test classes follows the same proportions as in ActivityNet1.3. Due to the scarcity of single-instance videos in the original THUMOS14 data, we divide the multi-instance video into non-overlapping snippets, each of which will be regarded as a new single-instance video. Under the multi-instance setting, we continue to use the initial video from THUMOS14, the same as we did for ActivityNet1.3.

Human-related Anomaly Localization (HAL) Dataset is our newly-collected dataset, which contains 1,161 videos and 12 types of human-related anomalous behaviors, as shown in Figure 4 and 5. For the few-shot learning setup, we follow the same class splitting protocol as with ActivityNet1.3, dividing the 12 anomaly classes into training, validation, and test sets. As illustrated in the statistical analysis in Figure 4c, the anomalous events in our HAL dataset are inherently sparse, with most videos containing only one or two distinct anomaly segments. Therefore, we utilize the original videos for all experiments on the HAL dataset without making a distinction between single-instance and multi-instance scenarios.

Evaluation Metrics. We utilize the mean average precision (mAP) as an evaluation metric to assess the performance of our method, consistent with prior state-of-the-art work [19], and report mAP at an IoU threshold of 0.5.

B. Implementation Details

We adopt the Adam optimizer [68] with the learning rate of $5e-6$ for ActivityNet1.3 and $1e-6$ for THUMOS14 and HAL, implemented in the PyTorch [69] framework on a NVIDIA A6000 GPU. During video feature extraction, we rescale the video feature sequences to $T = 100$ snippets for ActivityNet1.3, $T = 256$ for THUMOS14, and $T = 512$ for HAL using linear interpolation. For ActivityNet1.3, we train 200 epochs and the batch size is set to 100 with 100 episodes per epoch. For THUMOS14, we train 100 epochs and the batch size is set to 20 with 50 episodes per epoch. For HAL, we train 150 epochs and the batch size is set to 30 with 50 episodes per epoch.

C. Comparison with State-of-the-Art Methods

We compare our method with the state-of-the-art few-shot TAL methods [14]–[19], [44], [67] on ActivityNet1.3 and THUMOS14 datasets in Table I. Additionally, we conduct experiments on the HAL dataset and report in the Table III (a).

ActivityNet1.3. Our method consistently outperforms existing few-shot TAL methods in single-instance and multi-instance scenarios across 1-shot and 5-shot settings. In the multi-instance 5-shot case, it achieves 58.7 mAP@0.5, while in the single-instance 1-shot setting, it reaches 71.5 mAP@0.5. This performance can be attributed to two key factors: First, we extract hierarchical features from temporal and semantic dimensions, allowing better localization of action regions and enhancing semantic relationships. Additionally, incorporating textual information improves the model’s ability to capture

TABLE I
COMPARISON WITH STATE-OF-THE-ART METHODS IN TERMS OF MAP@0.5 ON ACTIVITYNET1.3 AND THUMOS14 DATASETS, UNDER SINGLE-INSTANCE AND MULTI-INSTANCE SETTINGS. THE BEST RESULTS ARE HIGHLIGHTED IN **BOLD**, AND THE SECOND-BEST RESULTS ARE UNDERLINED.

Method	ActivityNet1.3				THUMOS14			
	Single-instance		Multi-instance		Single-instance		Multi-instance	
	1-shot	5-shot	1-shot	5-shot	1-shot	5-shot	1-shot	5-shot
Video Re-localization [67]	43.5	-	31.4	-	34.1	-	4.3	-
Silco [17]	41.0	45.4	29.6	38.9	-	42.2	-	6.8
Common Action Localization [14]	53.1	56.5	42.1	43.9	48.7	51.9	7.5	8.6
Few-shot Transformer [15]	57.5	60.6	47.8	48.7	-	-	-	-
QAT [16]	55.6	63.8	44.9	51.8	51.2	56.1	9.1	13.8
ABA [18]	60.7	61.2	-	-	-	-	-	-
CDC-CA [19]	63.1	<u>67.5</u>	<u>49.4</u>	<u>54.6</u>	<u>55.0</u>	60.5	<u>10.2</u>	<u>16.2</u>
CGCN [44]	<u>66.6</u>	67.2	-	-	58.1	60.1	-	-
Ours	69.6	71.5	54.9	58.7	54.1	62.6	14.1	18.2

class variations and commonalities, further enhancing alignment and localization.

THUMOS14. As shown in Table I, our method achieves competitive results across various settings, particularly in the multi-instance 1-shot and 5-shot scenarios, where it improves upon [19] by 38.2% and 12.3%, respectively. In the single-instance 1-shot scenario, mAP@0.5 declines because the single-instance snippets in THUMOS14 are individually extracted from multi-instance videos. Each snippet has an incomplete action and a short duration, which hinders our CoE text from providing comprehensive guidance on action sequences.

HAL. Table III (a) presents our results on our collected HAL dataset. As shown in the table, our method outperforms [44] by 2.9 in mAP@0.5 and by 6.5 in mean mAP under the 5-shot scenario. This improvement can be attributed to the CoE text, which provides a comprehensive logical process for the occurrence of abnormal events, thereby assisting the model in accurately locating the anomalous snippets, where the behavioral logic analysis determines abnormality through temporal patterns, contextual correlations, and scene intentions.

D. Ablation Study

Impact of Different Components. We evaluate the impact of different components of our method under a multi-instance scenario on THUMOS14 in Table II. First, we establish our base model by removing the STPE and all operations involving text. Subsequently, we gradually add the STPE and textual information to the base. As shown in the table, the results improve with the addition of different modules, demonstrating the effectiveness of the various components proposed in this paper.

Impact of Semantic-Temporal Pyramid Encoder. We evaluate the impact of different variants of STPE in Table III (b). The following variants are considered: 1) *w/o STPE*: remove the STPE and use only the backbone; 2) *w/o TP*: utilize only the semantic pyramid block; 3) *w/o SP*: utilize only the temporal pyramid block; 4) *Transformer*: replace STPE with Transformer [70], which has comparable parameters for

TABLE II
THE IMPACT OF DIFFERENT COMPONENTS.

Method	STPE	Text	Multi-instance	
			1-shot	5-shot
Base			7.6	10.6
Base + STPE	✓		8.6	13.0
Base + Text		✓	13.0	14.6
Ours	✓	✓	14.1	18.2

feature extraction. The results indicate that removing the semantic or temporal pyramid block leads to a decrease in performance. Notably, completely removing STPE causes a significant drop. In comparison, our approach outperforms Transformer, demonstrating that robust feature extraction from both semantic and temporal dimensions significantly enhances localization performance.

Impact of Different Textual Content. We compare our text generation approach with alternative methods in Table III (c). The following text categories are evaluated: 1) *Prompt*: category-based prompts, e.g., “A video of class basketball dunk”; 2) *Caption*: frame-level captions generated by CoCa [71]; 3) *Video description*: detailed descriptions produced by VideoChat [20]; 4) *CoE Text**: the CoE text solely produced by VideoChat. Among the evaluated methods, *prompt* lacks specificity regarding video content, while *caption* fails to capture long-term temporal dependencies within the action sequence. Although *video description* provides temporal information, it often introduces noises through redundant environment details. Since VideoChat is not a reasoning model, *CoE Text** cannot effectively uncover logical relationships, resulting in lower quality of the generated CoE text. In contrast, our proposed CoE Text generated by VLM and LLM effectively extracts relevant context and exploits both temporal and causal relationships, thereby enhancing cross-modal alignment and localization accuracy. As demonstrated in Table III (c), our method consistently outperforms other approaches across multiple evaluation metrics.

Impact of Semantic-Aware Text-Visual Alignment. We

TABLE III
MAIN RESULT ON THE HAL DATASET AND ABLATION STUDY ON THE THUMOS14 DATASET.

Method	1-shot		5-shot	
	0.5	Mean	0.5	Mean
(a) Main Results on HAL dataset				
Base	5.9	2.6	14.6	8.1
Transformer	32.4	20.4	34.6	21.2
CGCN	36.3	19.8	37.1	20.2
Ours (on HAL)	38.9	25.2	40.0	26.7
(b) Impact of Semantic-Temporal Pyramid Encoder				
w/o STPE	13.0	4.2	14.6	4.9
w/o TP	13.5	4.2	17.1	5.0
w/o SP	13.7	4.8	17.6	5.5
Transformer	13.4	4.6	16.7	5.3
(c) Impact of Different Textual Content				
Prompt	12.5	3.4	14.5	5.3
Caption	12.9	4.6	16.4	5.4
Description	13.1	4.5	16.6	5.5
CoE Text*	13.3	4.6	16.9	5.6
(d) Impact of Semantic-Aware Text-Visual Alignment				
<i>Alignment Similarity Metric</i>				
Euclidean	11.5	4.3	14.5	5.3
Manhattan	13.5	5.3	17.7	6.2
<i>Alignment Strategy</i>				
VV (Video-Video Only)	11.3	3.5	13.8	4.2
VT (Video-Text Only)	12.4	4.9	13.4	5.3
VV+VT (Summation)	12.7	4.0	15.8	4.8
Ours (on THUMOS14)	14.1	5.4	18.2	7.3

conduct a comprehensive ablation study on the choice of similarity metric and the alignment strategies, with the results presented in Table III (d). First, we evaluate different metrics for computing the alignment maps between query and support features. We compare cosine similarity against two other common distance measures: Euclidean and Manhattan distances. The experimental results clearly show that cosine similarity significantly outperforms the other two. This is likely because it focuses on the orientation of the feature vectors (*i.e.*, semantic content) rather than their magnitude, making it more robust for capturing semantic relationships between features. Subsequently, we evaluate the impact of three different alignment strategies. 1) *VV*: align only the query video features with the support video features by operation \mathcal{S} ; 2) *VT*: align the query video features with support features that have been aligned with text by operation \mathcal{S} ; 3) *VV+VT*: combining both strategies (*VV* and *VT*) by summation. The results indicate that incorporating textual semantic information for alignment outperforms methods relying solely on video information. Among the strategies evaluated, our approach which leverages both video and text information yields the best results. Furthermore, using multiplication in our method is more effective than direct addition, as it refines the incorrect alignment in \mathcal{M}^v by multiplying it with the correct alignment score in \mathcal{M}^{vt} derived from the auxiliary textual information. In contrast, direct addition inherently accumulates misalignment errors, which degrade accuracy at higher IoU thresholds and consequently reduce the mAP.

Different Semantic Pyramid Layers and Semantic Nodes. We evaluate the impact of the number of semantic

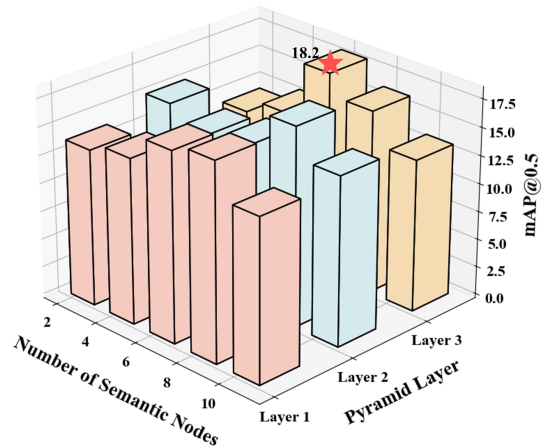


Fig. 7. Ablation study on the hyperparameters of the Semantic Pyramid: number of layers and semantic nodes. The best performance is marked with a red star.

TABLE IV
THE IMPACT OF DIFFERENT BACKBONES ON THE ACTIVITYNET1.3 DATASET.

Method	Single-instance		Multi-instance	
	1-shot	5-shot	1-shot	5-shot
Lee et al. [19]	63.1	67.5	49.4	54.6
Zhang et al. [44]	66.6	67.2	-	-
Ours (ViViT)	66.7	67.7	52.4	53.3
Ours (C3D+STPE)	69.6	71.5	54.9	58.7
Ours (ViViT+STPE)	71.3	75.1	58.6	60.1

pyramid layers and nodes (snippets) performing semantic attention operations at each layer within the Semantic-Temporal Pyramid Encoder (STPE). The results of mAP@0.5 under the multi-instance scenario of THUMOS14 are shown in Figure 7. We fix the number of STPE blocks to 2 and vary the number of pyramid layers for semantic attention operations to range from 1 to 3. When the number of layers is fixed, adding more semantic nodes leads to a gradual peak on mAP@0.5 before it starts to decline. This decline may result from the heightened likelihood of both foreground and background snippets simultaneously engaging in semantic attention operations, which diminishes the model’s ability to capture variance within the action and fails to distinguish between foreground and background snippets. Our proposed method achieves optimal performance when the number of semantic nodes is 6 and the number of layers is 3, as indicated by the red mark in Figure 7.

Impact of Different Backbones. To ensure a fair comparison with prior works, we adopt the conventional C3D [54] as the backbone for our main experiments. Moreover, we also conduct an additional evaluation on the ActivityNet1.3 dataset using a more advanced Transformer-based backbone, ViViT [72], with the mAP@0.50 results presented in Table IV. As the table shows, merely replacing the backbone with ViViT already establishes a strong baseline. Crucially, when our STPE module is further applied on the features extracted by ViViT, the performance is significantly enhanced across all settings. The results not only validate the direct benefits of

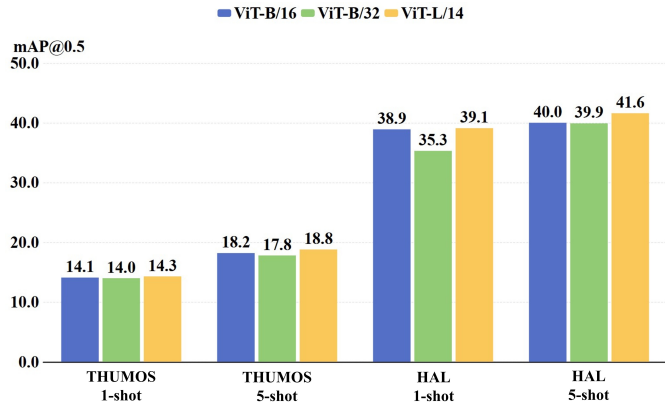


Fig. 8. The impact of different CLIP variants compared across the THUMOS14 and HAL datasets.

TABLE V

THE IMPACT OF DIFFERENT VLMS AND LLMs ON THE THUMOS14 AND HAL DATASETS. “*” DENOTES REASONING MODEL AND “Q” REPRESENTS “QWEN”.

VLM	LLM	THUMOS14		HAL					
		1-shot	5-shot	1-shot	5-shot				
		0.5	Mean	0.5	Mean				
Q2.5-VL 7B	Q3-30B(no think)	13.4	4.2	14.1	4.0	38.0	23.6	39.3	24.3
	Q3-30B(think)*	14.9	4.3	18.7	5.8	39.5	23.8	41.3	24.8
VideoChat 7B	Q3-30B(no think)	14.3	4.0	15.0	4.6	38.1	25.1	38.9	24.0
	Q3-30B(think)*	14.6	4.3	18.8	5.9	39.9	24.1	42.6	27.0
	Q2.5-Max	13.0	4.0	15.1	4.4	37.8	24.6	39.9	25.4
	DeepSeek-R1-70B*	14.1	5.4	18.2	7.3	38.9	25.2	40.0	26.7

using a superior backbone, but also indirectly demonstrate the effectiveness of our proposed STPE module.

Impact of CLIP. We evaluate the impact of different CLIP models on the localization performance. With the VLM and LLM fixed as VideoChat and DeepSeek-R1, we employ three CLIP models: clip-vit-base-patch16, clip-vit-base-patch32, and clip-vit-large-patch14 to perform textual encoding of both frame-level captions and CoE texts. The results of mAP@0.5 under the multi-instance scenario of THUMOS14 and HAL datasets are shown in Figure 8. The clip-vit-base-patch16 captures finer visual details and achieves more granular alignment in CLIP’s semantic space than clip-vit-base-patch32. Its text encoder better captures detailed textual descriptions and maps them to the semantic alignment space, assisting the visual model in detecting subtle actions and thereby improving performance. Although the larger CLIP model achieves slightly better performance on certain metrics, its overall effectiveness is comparable to or even inferior to that of clip-vit-base-patch16, especially when considering the higher resource consumption. Therefore, we adopt clip-vit-base-patch16 as the default CLIP model in subsequent experiments.

Impact of VLMS and LLMs. With CLIP fixed as clip-vit-base-patch16, we conduct a comparative analysis of the impact of different VLMS and LLMs on overall performance. For the VLM, we select Qwen2.5-VL-7B-Instruct [22] and VideoChat-Flash-Qwen2-7B-res448 [20]; for the LLM, we choose Qwen3-30B-A3B [73], DeepSeek-R1-Distill-Llama-

70B [52] and Qwen2.5-Max [74]. Among these LLMs, Qwen3-30B-A3B supports dynamic switching between standard and reasoning modes during inference. When operating in reasoning mode, it is considered a reasoning model. All reasoning models are marked with a *. We conduct experiments on the THUMOS14 and HAL datasets under the multi-instance scenario, and report the mAP@0.5 and mean mAP results for both 1-shot and 5-shot settings in Table V. As shown in the table, reasoning models consistently outperform non-reasoning models, and the reasoning capability of the LLM has a more significant impact on performance than the choice of VLM. For instance, Qwen3-30B-A3B achieves better results in reasoning (think) mode than in standard (no think) mode, demonstrating the positive effect of reasoning-based text generation. Moreover, despite having fewer parameters, DeepSeek-R1-Distill-Llama-70B outperforms Qwen-Max, further validating that reasoning-generated text can more effectively enhance model performance.

E. Qualitative analysis.

To prove the effectiveness of our method, we show qualitative results of one case from the ActivityNet1.3 in Figure 9a and one case from the HAL dataset in Figure 9b. We observe that our method locates the action snippets more accurately than QAT [16] under a 5-shot setting and maintains comparable performance under the 1-shot setting. This improvement is largely attributed to our CoE reasoning. Unlike the standard caption that describes an isolated state, our CoE text explicitly expresses the causal relation and the evidence of the anomaly by logical connectors (like “causing” and “leads to” as Figure 9b shows). This structured CoE text serves as a semantic guide, enabling the model to logically connect sequential sub-events ($e_i \rightarrow e_{i+1}$) and identify the critical start and end of the anomaly, thus resulting in more precise temporal boundaries compared to the baseline.

VI. CONCLUSION

In this paper, we presented a novel few-shot TAL method to enhance localization performance by integrating textual semantic information. First, we designed a CoE reasoning method to generate textual descriptions that can express temporal dependencies and causal relationships between actions. Then, a novel few-shot learning framework was designed to capture hierarchical action commonalities and variations by aligning query and support videos. Extensive experiments demonstrate the effectiveness and superiority of our proposed method. In the future, we will leverage our proposed method into more vertical fields, such as social security governance.

REFERENCES

- [1] Z. Shou, D. Wang, and S.-F. Chang, “Temporal action localization in untrimmed videos via multi-stage cnns,” in *2016 IEEE Conference on Computer Vision and Pattern Recognition (CVPR)*, 2016, pp. 1049–1058.
- [2] Y. Zhao, Y. Xiong, L. Wang, Z. Wu, X. Tang, and D. Lin, “Temporal action detection with structured segment networks,” in *Proceedings of the IEEE International Conference on Computer Vision*, 2017, pp. 2914–2923.

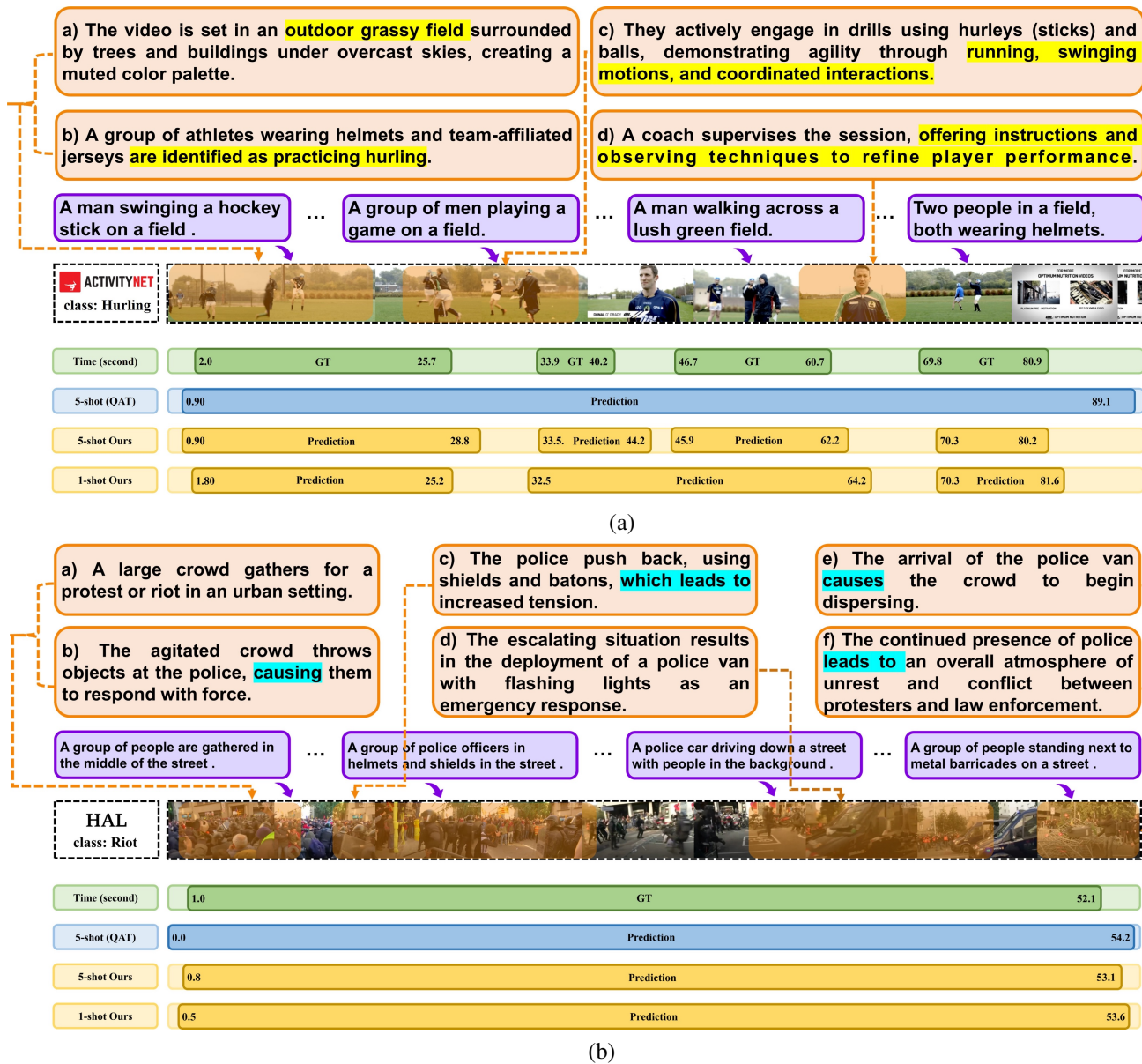


Fig. 9. Qualitative comparisons of our method against QAT [16] and Ground Truth. Purple boxes denote standard captions, and orange boxes represent our generated CoE text. (a) Visual results on “Hurling” from ActivityNet 1.3. While standard captions provide only brief descriptions, the CoE text offers a comprehensive narrative that better defines the action context. (b) Visual results on “Riot” from the HAL dataset. Unlike captions that only offer static descriptions, the CoE text captures the more meaningful causal relation (highlighted in cyan, e.g., “causing”, “leads to”) of the anomaly. This casual CoE text enables our model to align complex visual features with semantic information, resulting in more precise localization compared to QAT [16].

- [3] S. Buch, V. Escorcia, C. Shen, B. Ghanem, and J. C. Niebles, “Sst: Single-stream temporal action proposals,” in *2017 IEEE Conference on Computer Vision and Pattern Recognition (CVPR)*, 2017, pp. 6373–6382.
- [4] J. Tan, J. Tang, L. Wang, and G. Wu, “Relaxed transformer decoders for direct action proposal generation,” in *Proceedings of the IEEE/CVF International Conference on Computer Vision (ICCV)*, October 2021, pp. 13 526–13 535.
- [5] T. Lin, X. Zhao, and Z. Shou, “Single shot temporal action detection,” in *Proceedings of the 25th ACM International Conference on Multimedia*, ser. MM ’17. New York, NY, USA: Association for Computing Machinery, 2017, p. 988–996. [Online]. Available: <https://doi.org/10.1145/3123266.3123343>
- [6] M. Xu, C. Zhao, D. S. Rojas, A. Thabet, and B. Ghanem, “G-tad: Sub-graph localization for temporal action detection,” in *2020 IEEE/CVF Conference on Computer Vision and Pattern Recognition (CVPR)*, 2020, pp. 10 153–10 162.
- [7] C.-L. Zhang, J. Wu, and Y. Li, “Actionformer: Localizing moments of actions with transformers,” in *European Conference on Computer Vision*, ser. LNCS, vol. 13664, 2022, pp. 492–510.
- [8] K. Lee, S. Maji, A. Ravichandran, and S. Soatto, “Meta-learning with differentiable convex optimization,” in *2019 IEEE/CVF Conference on Computer Vision and Pattern Recognition (CVPR)*, 2019, pp. 10 649–10 657.
- [9] C. Finn, P. Abbeel, and S. Levine, “Model-agnostic meta-learning for fast adaptation of deep networks,” in *International conference on machine learning*. PMLR, 2017, pp. 1126–1135.
- [10] Y. Chen, Z. Liu, H. Xu, T. Darrell, and X. Wang, “Meta-baseline: Exploring simple meta-learning for few-shot learning,” in *Proceedings of the IEEE/CVF international conference on computer vision*, 2021, pp. 9062–9071.
- [11] Q. Sun, Y. Liu, T.-S. Chua, and B. Schiele, “Meta-transfer learning for few-shot learning,” in *2019 IEEE/CVF Conference on Computer Vision and Pattern Recognition (CVPR)*, 2019, pp. 403–412.
- [12] W.-Y. Chen, Y.-C. Liu, Z. Kira, Y.-C. F. Wang, and J.-B. Huang, “A closer look at few-shot classification,” *arXiv preprint arXiv:1904.04232*, 2019.
- [13] G. S. Dhillon, P. Chaudhari, A. Ravichandran, and S. Soatto, “A baseline

- for few-shot image classification,” *arXiv preprint arXiv:1909.02729*, 2019.
- [14] P. Yang, V. T. Hu, P. Mettes, and C. G. Snoek, “Localizing the common action among a few videos,” in *Computer Vision–ECCV 2020: 16th European Conference, Glasgow, UK, August 23–28, 2020, Proceedings, Part VII 16*. Springer, 2020, pp. 505–521.
- [15] P. Yang, P. Mettes, and C. G. Snoek, “Few-shot transformation of common actions into time and space,” in *Proceedings of the IEEE/CVF conference on computer vision and pattern recognition*, 2021, pp. 16 031–16 040.
- [16] S. Nag, X. Zhu, and T. Xiang, “Few-shot temporal action localization with query adaptive transformer,” *arXiv preprint arXiv:2110.10552*, 2021.
- [17] T. Hu, P. Mettes, J.-H. Huang, and C. G. Snoek, “Silco: Show a few images, localize the common object,” in *Proceedings of the IEEE/CVF International Conference on Computer Vision*, 2019, pp. 5067–5076.
- [18] H.-Y. Hsieh, D.-J. Chen, C.-W. Chang, and T.-L. Liu, “Aggregating bilateral attention for few-shot instance localization,” in *Proceedings of the IEEE/CVF Winter Conference on Applications of Computer Vision*, 2023, pp. 6325–6334.
- [19] J. Lee, M. Jain, and S. Yun, “Few-shot common action localization via cross-attentional fusion of context and temporal dynamics,” in *Proceedings of the IEEE/CVF International Conference on Computer Vision*, 2023, pp. 10 214–10 223.
- [20] X. Li, Y. Wang, J. Yu, X. Zeng, Y. Zhu, H. Huang, J. Gao, K. Li, Y. He, C. Wang *et al.*, “Videochat-flash: Hierarchical compression for long-context video modeling,” *arXiv preprint arXiv:2501.00574*, 2024.
- [21] Y. Wang, X. Li, Z. Yan, Y. He, J. Yu, X. Zeng, C. Wang, C. Ma, H. Huang, J. Gao *et al.*, “Internvideo2. 5: Empowering video mlms with long and rich context modeling,” *arXiv preprint arXiv:2501.12386*, 2025.
- [22] S. Bai, K. Chen, X. Liu, J. Wang *et al.*, “Qwen2.5-vl technical report,” *arXiv preprint arXiv:2502.13923*, 2025. [Online]. Available: <https://arxiv.org/abs/2502.13923>
- [23] B. Liberatori, A. Conti, P. Rota, Y. Wang, and E. Ricci, “Test-time zero-shot temporal action localization,” in *2024 IEEE/CVF Conference on Computer Vision and Pattern Recognition (CVPR)*, 2024, pp. 18 720–18 729.
- [24] L. Chen, X. Wei, J. Li, X. Dong, P. Zhang, Y. Zang, Z. Chen, H. Duan, Z. Tang, L. Yuan *et al.*, “Sharegpt4video: Improving video understanding and generation with better captions,” *Advances in Neural Information Processing Systems*, vol. 37, pp. 19 472–19 495, 2024.
- [25] T. Lin, X. Zhao, H. Su, C. Wang, and M. Yang, “Bsn: Boundary sensitive network for temporal action proposal generation,” in *Proceedings of the European Conference on Computer Vision (ECCV)*, September 2018.
- [26] R. Zeng, W. Huang, M. Tan, Y. Rong, P. Zhao, J. Huang, and C. Gan, “Graph convolutional networks for temporal action localization,” in *Proceedings of the IEEE/CVF International Conference on Computer Vision*, 2019, pp. 7094–7103.
- [27] F. Cheng and G. Bertasius, “Tallformer: Temporal action localization with a long-memory transformer,” in *Computer Vision – ECCV 2022*, S. Avidan, G. Brostow, M. Cissé, G. M. Farinella, and T. Hassner, Eds. Cham: Springer Nature Switzerland, 2022, pp. 503–521.
- [28] W. Yun, M. Qi, C. Wang, and H. Ma, “Weakly-supervised temporal action localization by inferring salient snippet-feature,” in *Proceedings of the AAAI conference on artificial intelligence*, vol. 38, no. 7, 2024, pp. 6908–6916.
- [29] M. Qi, H. Ye, J. Peng, and H. Ma, “Action quality assessment via hierarchical pose-guided multi-stage contrastive regression,” *IEEE Transactions on Image Processing*, vol. 34, pp. 6461–6474, 2025.
- [30] W. Deng, M. Qi, and H. Ma, “Global-local tree search in vlms for 3d indoor scene generation,” in *Proceedings of the Computer Vision and Pattern Recognition Conference*, 2025, pp. 8975–8984.
- [31] C. Lv, S. Zhang, Y. Tian, M. Qi, and H. Ma, “Disentangled counterfactual learning for physical audiovisual commonsense reasoning,” *Advances in Neural Information Processing Systems*, vol. 36, pp. 12 476–12 488, 2023.
- [32] M. Qi, W. Li, Z. Yang, Y. Wang, and J. Luo, “Attentive relational networks for mapping images to scene graphs,” in *Proceedings of the IEEE/CVF Conference on Computer Vision and Pattern Recognition*, 2019, pp. 3957–3966.
- [33] M. Qi, J. Qin, Y. Yang, Y. Wang, and J. Luo, “Semantics-aware spatial-temporal binaries for cross-modal video retrieval,” *IEEE Transactions on Image Processing*, vol. 30, pp. 2989–3004, 2021.
- [34] W. Yun, M. Qi, F. Peng, and H. Ma, “Semi-supervised teacher-reference-student architecture for action quality assessment,” in *European Conference on Computer Vision*. Springer, 2024, pp. 161–178.
- [35] M. Qi, Y. Wang, A. Li, and J. Luo, “Sports video captioning via attentive motion representation and group relationship modeling,” *IEEE Transactions on Circuits and Systems for Video Technology*, vol. 30, no. 8, pp. 2617–2633, 2019.
- [36] M. Qi, J. Qin, A. Li, Y. Wang, J. Luo, and L. Van Gool, “stagnet: An attentive semantic rnn for group activity recognition,” in *Proceedings of the European conference on computer vision (ECCV)*, 2018, pp. 101–117.
- [37] M. Qi, Y. Wang, A. Li, and J. Luo, “Stc-gan: Spatio-temporally coupled generative adversarial networks for predictive scene parsing,” *IEEE Transactions on Image Processing*, vol. 29, pp. 5420–5430, 2020.
- [38] M. Qi, C. Lv, and H. Ma, “Robust disentangled counterfactual learning for physical audiovisual commonsense reasoning,” *IEEE Transactions on Pattern Analysis and Machine Intelligence*, 2025.
- [39] R. Wang, M. Qi, Y. Shao, A. Zhou, and H. Ma, “Adversarial contrastive learning based physics-informed temporal networks for cuffless blood pressure estimation,” *IEEE Transactions on Mobile Computing*, 2025.
- [40] C. Lv, M. Qi, L. Liu, and H. Ma, “T2sg: Traffic topology scene graph for topology reasoning in autonomous driving,” in *Proceedings of the Computer Vision and Pattern Recognition Conference*, 2025, pp. 17 197–17 206.
- [41] H. Ye, M. Qi, Z. Liu, L. Liu, and H. Ma, “Safedriverag: Towards safe autonomous driving with knowledge graph-based retrieval-augmented generation,” in *Proceedings of the 33rd ACM International Conference on Multimedia*, 2025, pp. 11 170–11 178.
- [42] P. Zhu, M. Qi, X. Li, W. Li, and H. Ma, “Unsupervised self-driving attention prediction via uncertainty mining and knowledge embedding,” in *Proceedings of the IEEE/CVF International Conference on Computer Vision*, 2023, pp. 8558–8568.
- [43] K. Keisham, A. Jalali, J. Kim, and M. Lee, “Multi-level alignment for few-shot temporal action localization,” *Information Sciences*, vol. 650, p. 119618, 2023.
- [44] S. Zhang, H. Wang, L. Wang, X. Han, and Q. Tian, “Cgcn: context graph convolutional network for few-shot temporal action localization,” *Information Processing & Management*, vol. 62, no. 1, p. 103926, 2025.
- [45] J. Achiam, S. Adler, S. Agarwal, L. Ahmad, I. Akkaya, F. L. Aleman, D. Almeida, J. Altenschmidt, S. Altman, S. Anadkat *et al.*, “Gpt-4 technical report,” *arXiv preprint arXiv:2303.08774*, 2023.
- [46] T. Brown, B. Mann, N. Ryder, M. Subbiah, J. D. Kaplan, P. Dhariwal, A. Neelakantan, P. Shyam, G. Sastry, A. Askell *et al.*, “Language models are few-shot learners,” *Advances in neural information processing systems*, vol. 33, pp. 1877–1901, 2020.
- [47] H. Touvron, L. Martin, K. Stone *et al.*, “Llama 2: Open foundation and fine-tuned chat models,” *arXiv preprint arXiv:2307.09288*, 2023.
- [48] A. Grattafiori, A. Dubey, A. Jauhri *et al.*, “The llama 3 herd of models,” 2024. [Online]. Available: <https://arxiv.org/abs/2407.21783>
- [49] B. Li, Y. Zhang, D. Guo, R. Zhang, F. Li, H. Zhang, K. Zhang, P. Zhang, Y. Li, Z. Liu *et al.*, “Llava-onevision: Easy visual task transfer,” *arXiv preprint arXiv:2408.03326*, 2024.
- [50] B. Lin, Y. Ye, B. Zhu, J. Cui, M. Ning, P. Jin, and L. Yuan, “Video-llava: Learning united visual representation by alignment before projection,” *arXiv preprint arXiv:2311.10122*, 2023.
- [51] Z. Chen, J. Wu, W. Wang, W. Su, G. Chen, S. Xing, M. Zhong, Q. Zhang, X. Zhu, L. Lu *et al.*, “Internvl: Scaling up vision foundation models and aligning for generic visual-linguistic tasks,” in *Proceedings of the IEEE/CVF conference on computer vision and pattern recognition*, 2024, pp. 24 185–24 198.
- [52] D. Guo, D. Yang, H. Zhang, J. Song, R. Zhang, R. Xu, Q. Zhu, S. Ma, P. Wang, X. Bi *et al.*, “Deepseek-r1: Incentivizing reasoning capability in llms via reinforcement learning,” *arXiv preprint arXiv:2501.12948*, 2025.
- [53] J. Wei, X. Wang, D. Schuurmans, M. Bosma, F. Xia, E. Chi, Q. V. Le, D. Zhou *et al.*, “Chain-of-thought prompting elicits reasoning in large language models,” *Advances in neural information processing systems*, vol. 35, pp. 24 824–24 837, 2022.
- [54] D. Tran, L. Bourdev, R. Fergus, L. Torresani, and M. Paluri, “Learning spatiotemporal features with 3d convolutional networks,” in *2015 IEEE International Conference on Computer Vision (ICCV)*, 2015, pp. 4489–4497.
- [55] S. Liu, H. Yu, C. Liao, J. Li, W. Lin, A. X. Liu, and S. Dustdar, “Pyrformer: Low-complexity pyramidal attention for long-range time series modeling and forecasting,” in *International Conference on Learning Representations*, 2022. [Online]. Available: <https://openreview.net/forum?id=0EXmFzUn5I>
- [56] A. Radford, J. W. Kim, C. Hallacy, A. Ramesh, G. Goh, S. Agarwal, G. Sastry, A. Askell, P. Mishkin, J. Clark *et al.*, “Learning transferable

visual models from natural language supervision,” in *International conference on machine learning*. PMLR, 2021, pp. 8748–8763.

- [57] B. He, X. Yang, L. Kang, Z. Cheng, X. Zhou, and A. Shrivastava, “Asmloc: Action-aware segment modeling for weakly-supervised temporal action localization,” in *Proceedings of the IEEE/CVF conference on computer vision and pattern recognition*, 2022, pp. 13 925–13 935.
- [58] N. Bodla, B. Singh, R. Chellappa, and L. S. Davis, “Soft-nms–improving object detection with one line of code,” in *Proceedings of the IEEE international conference on computer vision*, 2017, pp. 5561–5569.
- [59] G. Li, D. Cheng, X. Ding, N. Wang, X. Wang, and X. Gao, “Boosting weakly-supervised temporal action localization with text information,” in *Proceedings of the IEEE/CVF conference on computer vision and pattern recognition*, 2023, pp. 10 648–10 657.
- [60] S. Paul, N. C. Mithun, and A. K. Roy-Chowdhury, “Text-based temporal localization of novel events,” in *European Conference on Computer Vision*. Springer, 2022, pp. 567–587.
- [61] F. C. Heilbron, V. Escorcia, B. Ghanem, and J. C. Niebles, “Activitynet: A large-scale video benchmark for human activity understanding,” in *Proceedings of the IEEE/CVF Conference on Computer Vision and Pattern Recognition*, 2015, pp. 961–970.
- [62] Y.-G. Jiang, J. Liu, A. R. Zamir, G. Toderici, I. Laptev, M. Shah, and R. Sukthankar, “Thumos challenge: Action recognition with a large number of classes,” 2014, <https://www.crcv.ucf.edu/THUMOS14/>.
- [63] D. Damen, H. Doughty, G. M. Farinella, A. Furnari, E. Kazakos, J. Ma, D. Moltisanti, J. Munro, T. Perrett, W. Price *et al.*, “Rescaling egocentric vision: Collection, pipeline and challenges for epic-kitchens-100,” *International Journal of Computer Vision*, vol. 130, no. 1, pp. 33–55, 2022.
- [64] L. Zhu, L. Wang, A. Raj, T. Gedeon, and C. Chen, “Advancing video anomaly detection: A concise review and a new dataset,” in *The Thirty-eighth Conference on Neural Information Processing Systems Datasets and Benchmarks Track*, 2024.
- [65] P. Wu, j. Liu, Y. Shi, Y. Sun, F. Shao, Z. Wu, and Z. Yang, “Not only look, but also listen: Learning multimodal violence detection under weak supervision,” in *European Conference on Computer Vision (ECCV)*, 2020.
- [66] H. Du, S. Zhang, B. Xie, G. Nan, J. Zhang, J. Xu, H. Liu, S. Leng, J. Liu, H. Fan, D. Huang, J. Feng, L. Chen, C. Zhang, X. Li, H. Zhang, J. Chen, Q. Cui, and X. Tao, “Uncovering what, why and how: A comprehensive benchmark for causation understanding of video anomaly,” in *2024 IEEE/CVF Conference on Computer Vision and Pattern Recognition (CVPR)*, 2024, pp. 18 793–18 803.
- [67] Y. Feng, L. Ma, W. Liu, T. Zhang, and J. Luo, “Video re-localization,” in *Proceedings of the European Conference on Computer Vision (ECCV)*, 2018, pp. 51–66.
- [68] D. P. Kingma and J. Ba, “Adam: A method for stochastic optimization,” *arXiv preprint arXiv:1412.6980*, 2014.
- [69] A. Paszke, S. Gross, F. Massa, A. Lerer, J. Bradbury, G. Chanan, T. Killeen, Z. Lin, N. Gimelshein, L. Antiga *et al.*, “Pytorch: An imperative style, high-performance deep learning library,” *Advances in Neural Information Processing Systems*, vol. 32, pp. 8026–8037, 2019.
- [70] A. Vaswani, N. Shazeer, N. Parmar, J. Uszkoreit, L. Jones, A. N. Gomez, Ł. Kaiser, and I. Polosukhin, “Attention is all you need,” in *Advances in neural information processing systems*. Long Beach, CA, USA: MIT, 2017, pp. 5998–6008.
- [71] J. Yu, Z. Wang, V. Vasudevan, L. Yeung, M. Seyedhosseini, and Y. Wu, “Coca: Contrastive captioners are image-text foundation models. arXiv 2022,” *arXiv preprint arXiv:2205.01917*, vol. 2, 2022.
- [72] A. Arnab, M. Dehghani, G. Heigold, C. Sun, M. Lučić, and C. Schmid, “Vivit: A video vision transformer,” in *Proceedings of the IEEE/CVF international conference on computer vision*, 2021, pp. 6836–6846.
- [73] A. Yang, A. Li, B. Yang, B. Zhang, B. Hui, B. Zheng, B. Yu, C. Gao, C. Huang, C. Lv *et al.*, “Qwen3 technical report,” *arXiv preprint arXiv:2505.09388*, 2025.
- [74] Q. Team, “Qwen2.5 technical report,” *arXiv preprint arXiv:2412.15115*, 2024.



Mengshi Qi (Member, IEEE) is currently a Professor with the Beijing University of Posts and Telecommunications, Beijing, China. He received the B.S. degree from the Beijing University of Posts and Telecommunications in 2012, and the M.S. and Ph.D. degrees in computer science from Beihang University, Beijing, China, in 2014 and 2019, respectively. He was a postdoctoral researcher with the CVLAB, EPFL, Switzerland from 2019 to 2021. His research interests include machine learning and computer vision, especially scene understanding, 3D reconstruction, and multimedia analysis. He has published more than 40 papers in top journals (such as IEEE TIP, TPAMI, TMM, TCSVT, TIFS) and top conferences (such as IEEE CVPR, ICCV, ECCV, ACM Multimedia, AAAI, NeurIPS). He also has served as Area Chair of ICME 2024-2025, Senior PC Member of AAAI 2023-2025 and IJCAI 2021/2023-2025, and the Guest Editor for IEEE Transactions on Multimedia.



Hongwei Ji is currently working toward the master’s degree at the Beijing University of Posts and Telecommunications, Beijing, China. His research interests include multimodal learning and its applications in computer vision, particularly temporal action localization.



Wulian Yun is currently pursuing a Ph.D. degree at Beijing University of Posts and Telecommunications, China. Her research interests include deep learning/machine learning and its applications in computer vision, especially temporal action localization and video understanding.



Xianlin Zhang is now a Associate Professor at Beijing University of Posts and Telecommunications, China. Her current research focuses on generative artificial intelligence and video analysis and understanding. She received her Ph.D. degree from Beijing University of Posts and Telecommunications in 2019. To date, she have authored or co-authored more than 20 publications in prestigious journals and conferences, including CVPR, TMM, PR, ACM TOMM.



Huadong Ma (Fellow, IEEE) received the B.S. degree in mathematics from Henan Normal University, Xinxiang, China, in 1984, the M.S. degree in computer science from the Shenyang Institute of Computing Technology, Chinese Academy of Science, China, in 1990, and the Ph.D. degree in computer science from the Institute of Computing Technology, Chinese Academy of Science, Beijing, China, in 1995. He is currently a Professor of School of Computer Science, Beijing University of Posts and Telecommunications, Beijing, China. From 1999 to 2000, he held a Visiting Position with the University of Michigan, Ann Arbor, MI, USA. His current research interests include Internet of Things, sensor networks, and multimedia computing. He has authored more than 300 papers in journals, such as ACM/IEEE Transactions or conferences, such as ACM MobiCom, ACM SIGCOMM, IEEE INFOCOM, and five books. He was the recipient of the Natural Science Award of the Ministry of Education, China, in 2017, 2019 Prize Paper Award of IEEE TRANSACTIONS ON MULTIMEDIA, 2018 Best Paper Award from IEEE MULTIMEDIA, Best Paper Award in IEEE ICPADS 2010, Best Student Paper Award in IEEE ICME 2016 for his coauthored papers, and National Funds for Distinguished Young Scientists in 2009. He was/is an Editorial Board Member of the IEEE TRANSACTIONS ON MULTIMEDIA, IEEE INTERNET OF THINGS JOURNAL, ACM Transactions on Internet of Things. He is the Chair of ACM SIGMOBILE China.

Supplementary for Chain-of-Evidence Multimodal Reasoning for Few-shot Temporal Action Localization

Mengshi Qi, *Member, IEEE*, Hongwei Ji, Wulian Yun, Xianlin Zhang, Huadong Ma, *Fellow, IEEE*

I. TRAINING AND INFERENCE PROCESSES

For a better understanding of our few-shot temporal action localization task, we present the training and testing processes below. For the training process, we first randomly select a class C from the training subset D_{train} . Subsequently, we select $1 + K$ samples as query and support from C . For the support video, we generate caption text descriptions on each frame and CoE text descriptions via VLM and LLM. Then, we perform feature extraction on both the videos and the text. Specifically, for both the query video and each support video, we extract snippet features \mathcal{V}^q and \mathcal{V}^s using a fixed pre-trained backbone, and the corresponding support text is processed using the CLIP Text Encoder to extract features \mathcal{F}^{cap} and \mathcal{F}^{CoE} . These extracted video features are then passed through the STPE to further capture features \mathcal{F}^q and \mathcal{F}^s , text features \mathcal{F}^{cap} and \mathcal{F}^{CoE} are aligned through a cross-attention operation to generate the final text feature of the support set. Next, we align the support video features \mathcal{F}^s with the textual features \mathcal{F}^s by a video-text alignment block. Then, the query features \mathcal{F}^t , support features \mathcal{F}^s . The video-text aligned features $\mathcal{F}^{\hat{s}}$ are fed into a semantic-aware text-visual alignment module with Eq.(4) ~ Eq.(7) in our main paper. The aligned features are subsequently passed to the prediction head to perform action localization. Finally, we compute the loss through Eq.(8) ~ Eq.(10) in our main paper to optimize our model and update all parameters.

For the inference process, it is similar to the training process. The difference is that after obtaining the predictions, we need to select continuous snippets as proposals based on different thresholds in \mathcal{T} and then apply soft-NMS on all proposals. The training and testing processes are illustrated in the algorithms below.

II. COMPARED METHODS.

To validate the effectiveness of our proposed approach, we compare it with the following state-of-the-art methods: **1)** Feng *et al* [1] propose a cross-gated bilinear matching model; **2)** Hu *et al* [2] introduce a spatial similarity module combined with feature reweighting via graph convolutional networks; **3)** Yang *et al* [3] design a progressive alignment network to iteratively fuse support information into the query branch; **4)** Yang *et al* [4] propose a few-shot transformer architecture optimized for joint commonality learning and localization without proposals; **5)** Nag *et al* [5] introduce a query-adaptive

M. Qi, H. Ji, W. Yun, X. Zhang and H. Ma are with State Key Laboratory of Networking and Switching Technology, Beijing University of Posts and Telecommunications, China.

Algorithm 1 The Training Process of Our Method

Input: Training Dataset D_{train} , Epochs E , Episodes per Epoch N_{ep} , Shots K , Model M_θ
Output: Optimized Model M_θ

- 1: **for** $epoch = 1 \rightarrow E$ **do**
- 2: **for** $episode = 1 \rightarrow N_{ep}$ **do**
- 3: # Sample a task (episode)
- 4: Sample a class C from D_{train}
- 5: Sample query video \mathcal{V}^q and support set $\{\mathcal{V}_i^s\}_{i=1}^K$ from C
- 6: # Text Feature Extraction (offline)
- 7: Generate captions and CoE text for $\{\mathcal{V}_i^s\}$
- 8: $\mathcal{F}^{cap}, \mathcal{F}^{CoE} \leftarrow \text{CLIP-Text-Encoder}(\text{texts})$
- 9: # Forward Pass
- 10: $\mathcal{F}^q, \mathcal{F}^s \leftarrow \text{BackboneAndSTPE}(\mathcal{V}^q, \{\mathcal{V}_i^s\})$
- 11: $\mathcal{F}^t \leftarrow \text{CrossAttention}(\mathcal{F}^{cap}, \mathcal{F}^{CoE})$
- 12: $\mathcal{M}^v \leftarrow \text{CosineSimilarity}(\mathcal{F}^q, \mathcal{F}^s)$ # Eq. (4)
- 13: $\mathcal{F}^{\hat{s}} \leftarrow \text{Fuse}(\mathcal{F}^s, \mathcal{F}^t)$ # Eq. (5)
- 14: $\mathcal{M}^{vt} \leftarrow \text{CosineSimilarity}(\mathcal{F}^q, \mathcal{F}^{\hat{s}})$ # Eq. (6)
- 15: $\mathcal{M} \leftarrow \mathcal{M}^v \odot \mathcal{M}^{vt} \odot \mathcal{M}^m$ # Eq. (7)
- 16: $\hat{p} \leftarrow \text{PredictionHead}(\mathcal{M})$
- 17: # Compute Loss and Update Model
- 18: $\mathcal{L} \leftarrow \text{ComputeLoss}(\hat{p}, y^q)$ # Using Eq. (8-10)
- 19: Update model parameters θ by backpropagating \mathcal{L}
- 20: **end for**
- 21: **end for**

Algorithm 2 The Inference Process of Our Method

Input: Test Query Video \mathcal{V}^q , Support Set $\{\mathcal{V}_i^s, y_i^s\}_{i=1}^K$, Frozen Model M_θ , Confidence Threshold τ_{conf} , NMS Threshold τ_{nms}
Output: Final Action Proposals P_{final}

- 1: # Feature Extraction
- 2: Generate/Load captions and CoE text for $\{\mathcal{V}_i^s\}$
- 3: $\mathcal{F}^{cap}, \mathcal{F}^{CoE} \leftarrow \text{CLIP-Text-Encoder}(\text{texts})$
- 4: $\mathcal{F}^q, \mathcal{F}^s \leftarrow \text{BackboneAndSTPE}(\mathcal{V}^q, \{\mathcal{V}_i^s\})$
- 5: $\mathcal{F}^t \leftarrow \text{CrossAttention}(\mathcal{F}^{cap}, \mathcal{F}^{CoE})$
- 6: # Compute Snippet-level Probabilities
- 7: $\mathcal{M}^v \leftarrow \text{CosineSimilarity}(\mathcal{F}^q, \mathcal{F}^s)$
- 8: $\mathcal{F}^{\hat{s}} \leftarrow \text{Fuse}(\mathcal{F}^s, \mathcal{F}^t)$
- 9: $\mathcal{M}^{vt} \leftarrow \text{CosineSimilarity}(\mathcal{F}^q, \mathcal{F}^{\hat{s}})$
- 10: $\mathcal{M}^m \leftarrow \text{GenerateBackgroundMask}(\{y_i^s\})$
- 11: $\mathcal{M} \leftarrow \mathcal{M}^v \odot \mathcal{M}^{vt} \odot \mathcal{M}^m$
- 12: $\hat{p} \leftarrow \text{PredictionHead}(\mathcal{M})$ # Snippet-level probabilities
- 13: # Generate Proposals
- 14: $P_{raw} \leftarrow \emptyset$ # Initialize raw proposal set
- 15: Identify consecutive snippets in \mathcal{V}^q where probabilities $\hat{p} > \tau_{conf}$
- 16: Add identified snippets as proposals to P_{raw}
- 17: Filter out proposals that are too short
- 18: # Refine Proposals
- 19: $P_{final} \leftarrow \text{Soft-NMS}(P_{raw}, \tau_{nms})$
- 20: **return** P_{final}

Transformer capable of adapting to new classes; **6)** Hsieh *et al* [6] propose an Aggregating Bilateral Attention mechanism that uncovers query-support dependencies through embedding norms and context awareness; **7)** Lee *et al* [7] develop a cross-

Algorithm 3 Pipeline for Generating and Verifying CoE Text

Input: Video \mathcal{V} , VLM M_{vlm} , LLM M_{llm} , CLIP Textual Encoder M_{ct} , CLIP Visual Encoder M_{cv} , Prompts Library $\mathcal{P}_{1,2,3}$, Max Retries N_{retry} , Threshold α

Output: Verified CoE text o_3

- 1: # — Stage 1: Generate and Verify Detailed Description —
- 2: $p_1 \leftarrow \text{SelectPrompt}(\mathcal{P}_1)$, $x_0 \leftarrow \mathcal{V}$
- 3: $o_1 \leftarrow \text{GenerateAndVerify}(p_1, M_{vlm}, \alpha, N_{retry}, \text{context} = x_0)$
- 4: **if** o_1 is marked for human review **then return** Failure
- 5: **end if**
- 6: # — Stage 2: Extract and Verify Key Events —
- 7: $p_2 \leftarrow \text{SelectPrompt}(\mathcal{P}_2)$, $x_1 \leftarrow o_1$
- 8: $o_2 \leftarrow \text{GenerateAndVerify}(p_2, M_{vlm}, \alpha, N_{retry}, \text{context} = x_1)$
- 9: **if** o_2 is marked for human review **then return** Failure
- 10: **end if**
- 11: # — Stage 3: Generate and Verify CoE Text —
- 12: $p_3 \leftarrow \text{SelectPrompt}(\mathcal{P}_3)$, $x_2 \leftarrow \{o_1, o_2\}$
- 13: $o_3 \leftarrow \text{GenerateAndVerify}(p_3, M_{llm}, \alpha, N_{retry}, \text{context} = x_2)$
- 14: **return** o_3

- 15: **procedure** AUTOFILTER(Text o)
- 16: **if** o is too short or repeat **then**
- 17: **return** False
- 18: **end if**
- 19: **return** True
- 20: **end procedure**

- 21: **procedure** VERIFY(Video \mathcal{V} , Text o , Threshold α)
- 22: **if** not AutoFilter(o) **then**
- 23: **return** (False, {too short or repeat})
- 24: **end if**
- 25: $C \leftarrow \text{ParseText}(o)$; $F \leftarrow \text{SampleFrames}(\mathcal{V})$
- 26: $S \leftarrow \text{CosineSimilarity}(M_{ct}(C), M_{cv}(F))$
- 27: **for all** sub-sentence $c_j \in C$ **do**
- 28: **if** Average(TopK($S[j, :]$, $K = 3$)) $< \alpha$ **then**
- 29: **return** (False, {problematic sub-sentences})
- 30: **end if**
- 31: **end for**
- 32: **return** (True, \emptyset)
- 33: **end procedure**

- 34: **procedure** GENERATEANDVERIFY(Prompt p , Model M , α , N_{retry} , context=None)
- 35: **for** $i = 1 \rightarrow N_{retry}$ **do**
- 36: $o \leftarrow M(p, \text{context})$
- 37: is_consistent, issues $\leftarrow \text{VERIFY}(\mathcal{V}, o, \alpha)$
- 38: **if** is_consistent **then**
- 39: **return** o
- 40: **else**
- 41: $p \leftarrow \text{CreateRefinementPrompt}(p, \text{issues})$
- 42: **end if**
- 43: **end for**
- 44: **return** HumanReviewQueue.add(\mathcal{V}, o)
- 45: **end procedure**

correlation attention mechanism to transform support features into the query context; **8)** Zhang *et al* [8] propose the Context Graph Convolutional Network and utilize the multi-scale graph convolutions to model sequence, intra-action, and inter-action relationships.

III. MORE DETAILS ABOUT THE HAL DATASET

A. More Information about the Anomaly Types

In our HAL dataset, there are a total of 12 human-related anomaly categories, which are as follows: Animal Attack,

Assault, Abuse, Fighting, People Falling, Public Safety, Pedestrian Incidents, Robbery, Riot, Shooting, Social Unrest, Theft, and Vandalism. The specific quantities and the proportions are shown in Table I.

TABLE I
THE NUMBER OF VIDEOS FOR EACH ANOMALY TYPE BASED ON THE PROVIDED DATA.

Anomaly Type	Number
Robbery	235
Fighting	211
Shooting	153
Riot	129
Vandalism	84
Theft	83
Animal Attack	56
People Falling	43
Pedestrian Incidents	40
Assault	20
Abuse	11
Setting Fire	7
Total	1072

B. More visual examples of the HAL dataset

The HAL dataset features a diverse range of scene types, including stores, streets, private residences, trains, and more. Additionally, the video formats are varied, encompassing surveillance footage, news reports, short videos, and cinematic scenes. In Figure 1, we present more visuals to facilitate the observation of abnormal events across different scenes and video types. This diversity not only enhances the richness of the dataset but also provides a solid training foundation for the model’s generalization capabilities. By training the model with abnormal events in different scenes, we hope to further improve the model’s ability to detect anomalous behaviours in complex environments.

C. More CoE text examples of the HAL dataset

We not only generated frame-level descriptions but also more comprehensive CoE text for the HAL dataset. We selected six types of anomalies from the dataset and presented their corresponding CoE text in Figure 2 ~ Figure 4. Compared to captions, CoE text can more comprehensively express the complete process of anomalous events and provide more comprehensive textual guidance, thereby enhancing the accuracy of action localization.

D. Human evaluation of the CoE text quality

Beyond factual accuracy, the core advantage of CoE text lies in its logical coherence and inferential completeness. To quantitatively evaluate the quality of our generated text in these aspects, we conducted a human evaluation study. In this study, we compared the outputs of our method (VideoChat + DeepSeek-R1) against text generated by two baseline approaches: a powerful standalone VLM (Qwen2.5-VL-72B-AWQ) and a VLM+LLM combination (Qwen2.5-VL-7B + Qwen3-30B).

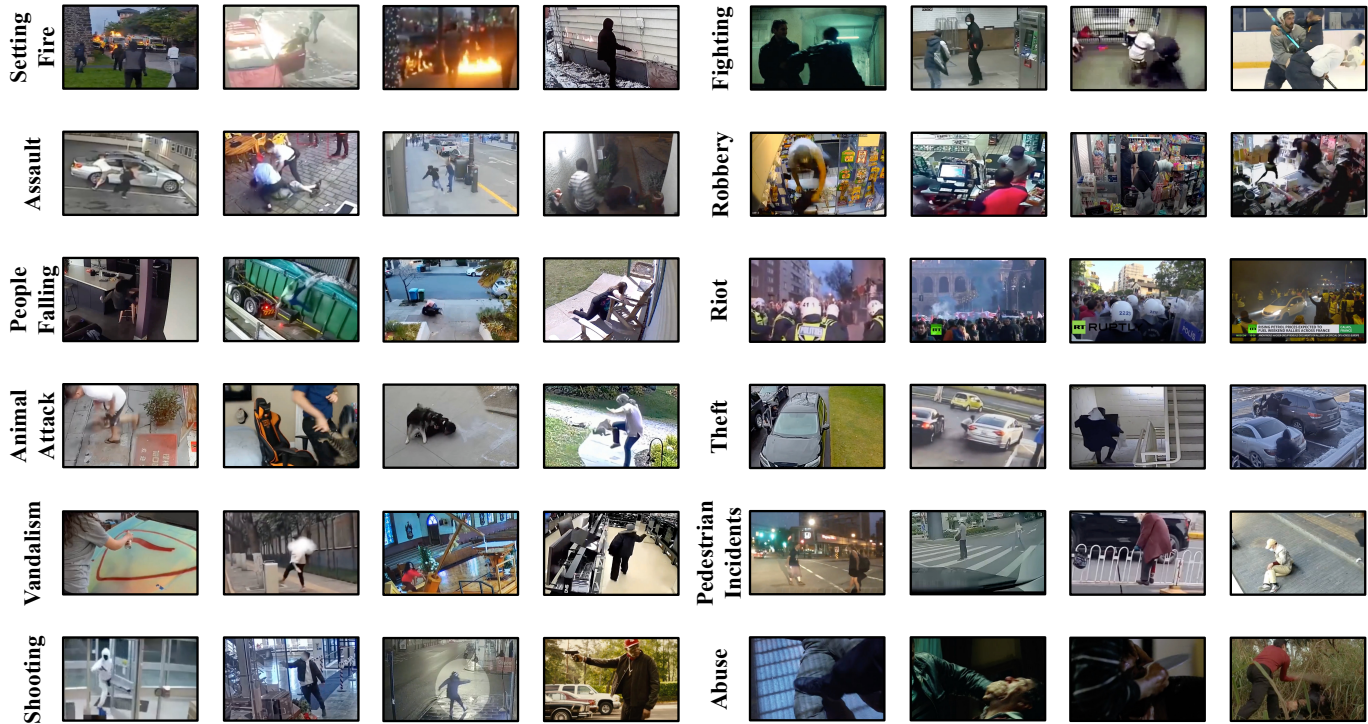


Fig. 1. The video samples include instances of different categories.

TABLE II
HUMAN EVALUATION OF CoT TEXT QUALITY, WITH A LOWER AVERAGE RANK INDICATING HIGHER QUALITY AND PREFERENCE.

Method	Average Rank ↓
Qwen2.5-VL-72B-AWQ	2.27
Qwen2.5-VL-7B + Qwen3-30B	2.09
Ours (VideoChat + DeepSeek-R1)	1.64

Our evaluation protocol involved 10 human participants who were asked to rank the outputs from the three methods based on four key criteria: 1) **Logical Soundness**: Is each step of the reasoning logical? 2) **Factuality**: Is the reasoning grounded in facts from the video? 3) **Completeness**: Are any key reasoning steps missing? 4) **Conciseness**: Are there unnecessary or redundant reasoning steps?

The results, summarized in Table II, clearly demonstrate the superiority of our method. In the side-by-side ranking, the CoE text generated by our approach was strongly preferred by human evaluators, achieving a superior average rank of 1.64. This significantly outperforms the baselines, which scored 2.09 and 2.27, respectively. This indicates that our stage-wise reasoning pipeline not only produces factually consistent text but also generates higher-quality output in terms of logic, completeness, and conciseness, providing a superior semantic guide for the subsequent localization task.

TABLE III
ABLATION STUDY OF THE NUMBER OF STPE BLOCKS.

Number of Blocks	1	2	3	4	5
mAP@0.5	14.5	18.2	16.6	13.2	11.9

IV. ADDITIONAL ABLATION AND VISUALIZATION ANALYSIS

A. Impact of the number of the STPE blocks

We analyze the impact of the number of STPE blocks on action localization performance. We fix the number of semantic nodes at 6 and the number of semantic pyramid layers at 3, conducting experiments under the multi-instance setting of THUMOS14, with results shown in Table III. Due to the limited number of video samples in the THUMOS14 dataset, the model cannot be adequately trained when the number of blocks exceeds 2, resulting in a decline in performance.

B. Visualization Analysis

To better illustrate the effectiveness of our method, we utilized T-SNE to visualize a sample from ActivityNet1.3 in Figure 5. The left side represents the original C3D features, while the right side shows the features after incorporating the STPE. Besides, we also select two sets of single-instance and multi-instance results from the ActivityNet1.3 dataset for visualization, one including correctly localized instances and the other containing incorrectly localized instances. We observe that in both sets of samples, QAT only achieves

relatively coarse localization, whereas our proposed method provides more accurate localization results, whether for 1-shot or 5-shot. Additionally, as shown in Figure 6~ Figure 8, our method achieves more consistent localization proposals under both multi-instance and single-instance scenarios, even when there are numerous short regions. In Figure 9 and Figure 10, we show several samples with localization errors (red background box). In these cases, our method incorrectly classifies some background snippets as foreground snippets. This may be due to the presence of similar foreground and background snippets in the original C3D snippet features or overly subtle action performers in ActivityNet1.3 videos. It leads to erroneous semantic attention operations in STPE, pushing these background snippets closer to the foreground snippets. Consequently, these background snippets are mistakenly localized as action regions during the post-processing phase.

REFERENCES

- [1] Y. Feng, L. Ma, W. Liu, T. Zhang, and J. Luo, "Video re-localization," in *Proceedings of the European Conference on Computer Vision (ECCV)*, 2018, pp. 51–66.
- [2] T. Hu, P. Mettes, J.-H. Huang, and C. G. Snoek, "Silco: Show a few images, localize the common object," in *Proceedings of the IEEE/CVF International Conference on Computer Vision*, 2019, pp. 5067–5076.
- [3] P. Yang, V. T. Hu, P. Mettes, and C. G. Snoek, "Localizing the common action among a few videos," in *Computer Vision–ECCV 2020: 16th European Conference, Glasgow, UK, August 23–28, 2020, Proceedings, Part VII 16*. Springer, 2020, pp. 505–521.
- [4] P. Yang, P. Mettes, and C. G. Snoek, "Few-shot transformation of common actions into time and space," in *Proceedings of the IEEE/CVF conference on computer vision and pattern recognition*, 2021, pp. 16 031–16 040.
- [5] S. Nag, X. Zhu, and T. Xiang, "Few-shot temporal action localization with query adaptive transformer," *arXiv preprint arXiv:2110.10552*, 2021.
- [6] H.-Y. Hsieh, D.-J. Chen, C.-W. Chang, and T.-L. Liu, "Aggregating bilateral attention for few-shot instance localization," in *Proceedings of the IEEE/CVF Winter Conference on Applications of Computer Vision*, 2023, pp. 6325–6334.
- [7] J. Lee, M. Jain, and S. Yun, "Few-shot common action localization via cross-attentional fusion of context and temporal dynamics," in *Proceedings of the IEEE/CVF International Conference on Computer Vision*, 2023, pp. 10 214–10 223.
- [8] S. Zhang, H. Wang, L. Wang, X. Han, and Q. Tian, "Cgcn: context graph convolutional network for few-shot temporal action localization," *Information Processing & Management*, vol. 62, no. 1, p. 103926, 2025.

Fighting



- a) A physical altercation occurs on a city street, where a man in a red shirt attacks another man who is lying on the ground and appears to be unconscious or incapacitated.
- b) This situation **leads to** two other men, one wearing black and the other wearing blue, intervening to stop the assault.
- c) Despite their intervention, the attacker continues to strike the man on the ground, **causing** further escalation of the confrontation.
- d) The persistent aggression of the attacker **results in** the two men restraining him to bring the situation under control.

People Falling



- a) A woman in a blue and white patterned top, denim shorts, and sandals attempts to climb over a wall using a chair for support, which **causes** her to hold onto the wall with one hand.
- b) Her unstable balance during the climbing process **leads to** her losing grip and falling off the chair.
- c) The fall **results in** her landing on the ground, completing the sequence of events.
- d) The timestamp (10:29 AM, October 30th, 2019) marks the occurrence of this incident.

Fig. 2. The CoE text of “Fighting” and “People Falling” anomaly type.

Robbery



- a) The store's interior, captured by a security camera, sets the scene with shelves and a counter area.
- b) Multiple individuals, some wearing hooded clothing, are present in the store.
- c) Their erratic movements and actions, such as throwing objects, **lead to** a chaotic atmosphere.
- d) Specific actions include a person in a green jacket running towards the counter and another in a black shirt standing near the entrance.
- e) These actions **result in** an overall disordered environment within the store.

Shooting



- a) A man in a blue jacket points a gun at another individual inside a white car at a gas station, creating a tense confrontation.
- b) This confrontation **leads to** the man in the blue jacket walking towards the white car and opening its door.
- c) His anger **causes** him to start shooting inside the car while shouting.
- d) The shooting **results in** smoke filling the air and a chaotic scene.
- e) The entire incident **leads to** an atmosphere of danger and urgency at the gas station.

Fig. 3. The CoE text of “Robbery” and “Shooting” anomaly type.

Assault



- a) A physical altercation breaks out between two individuals in a school hallway.
- b) The altercation **causes** a struggle on the floor, drawing the attention of bystanders.
- c) This **leads to** more people rushing to intervene and separate the combatants.
- d) **As a result**, a chaotic scene ensues with students and staff members gathering around.
- e) Amid the confusion, some individuals attempt to restrain the attackers while others observe from a distance.
- f) The tense atmosphere **causes** the crowd to disperse and regroup unpredictably.
- g) During this commotion, a person wearing a red shirt and black pants notices the situation.
- h) This **results in** the individual rushing toward the camera, possibly to get closer or assist.

Vandalism



- a) The video shows a surveillance camera view of the entrance to a building, where the scene is initially calm with no visible activity.
- b) An explosion suddenly occurs inside the building, **causing** significant damage to the glass doors and windows.
- c) The force of the blast shatters the glass, **leading to** debris scattering across the tiled floor in all directions.
- d) This **results** in a cloud of dust and disarray at the entrance area, with broken glass pieces scattered around.

Fig. 4. The CoE text of “Assault” and “Vandalism” anomaly type.

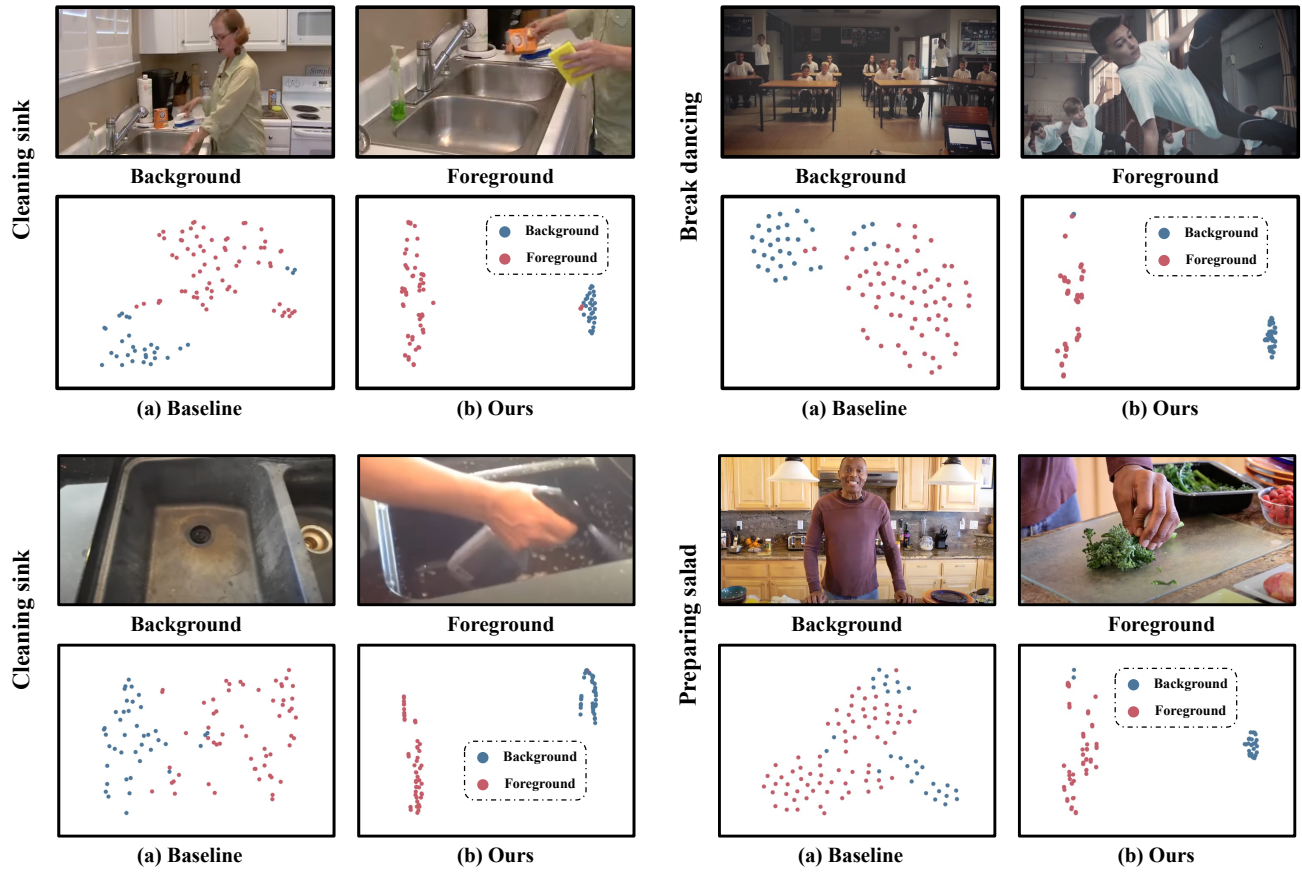


Fig. 5. T-SNE visualization of foreground and background features on “Cleaning sink”, “Break dancing” and “Preparing salad” of ActivityNet1.3 dataset. Red points and blue points denote foreground and background, respectively.

ACTIVITYNET Class: Cleaning sink											
Time (second)	5.0	9.2	11.7	19.1	21.1	GT				114.5	
5-shot (QAT)	2.4		Prediction							115.2	
5-shot Ours	2.4	8.2	10.6		Prediction				105.8		
1-shot Ours	2.4	10.6	13.0		Prediction				103.5		
ACTIVITYNET Class: Cleaning sink											
Time (second)	14.3	23.4	25.8		GT				163.1		
5-shot (QAT)	6.9		Prediction							163.7	
5-shot Ours	12.1	20.7	24.1		Prediction				153.5		
1-shot Ours	13.8	24.1	27.6		Prediction				158.6		

Fig. 6. Qualitative comparisons of our method (1-shot and 5-shot setting), QAT [5] (5-shot setting) and Ground Truth (GT) on “Cleaning sink (multi-instance)” of ActivityNet1.3 dataset.

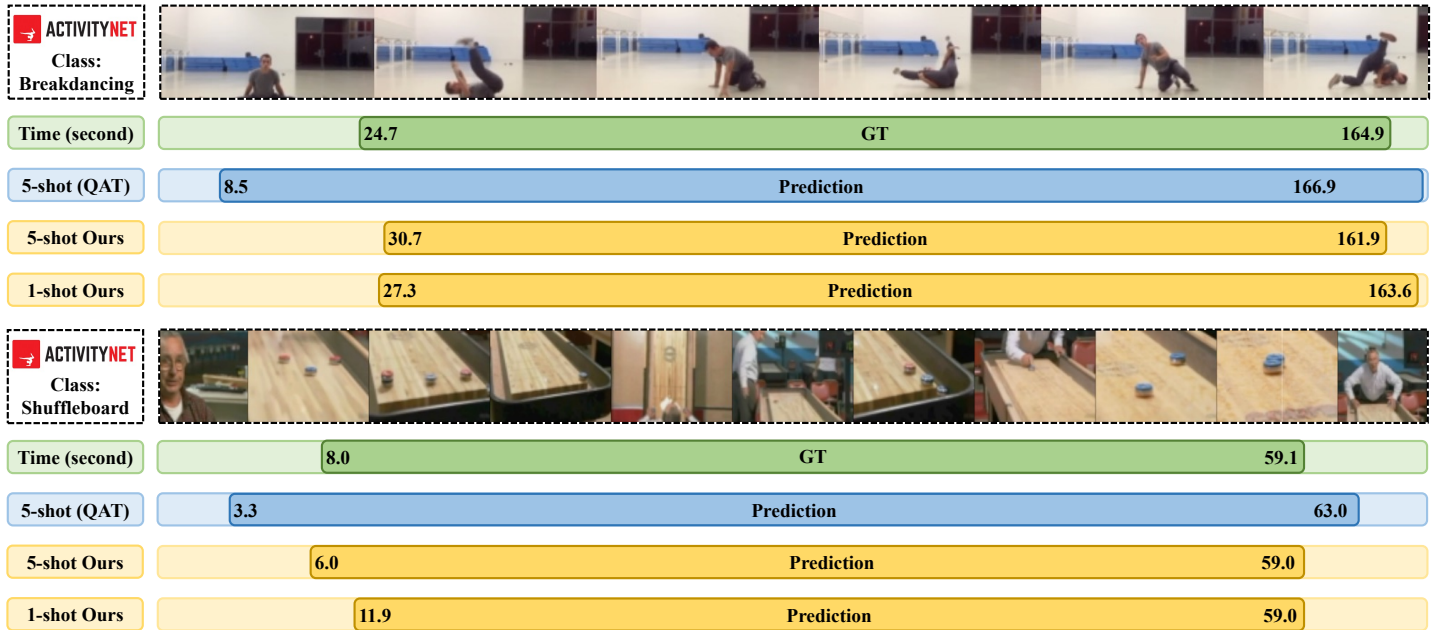


Fig. 7. Qualitative comparisons of our method (1-shot and 5-shot setting), QAT [5] (5-shot setting) and Ground Truth (GT) on “Breakdancing” (single-instance) and “Shuffleboard” (single-instance) of ActivityNet1.3 dataset.

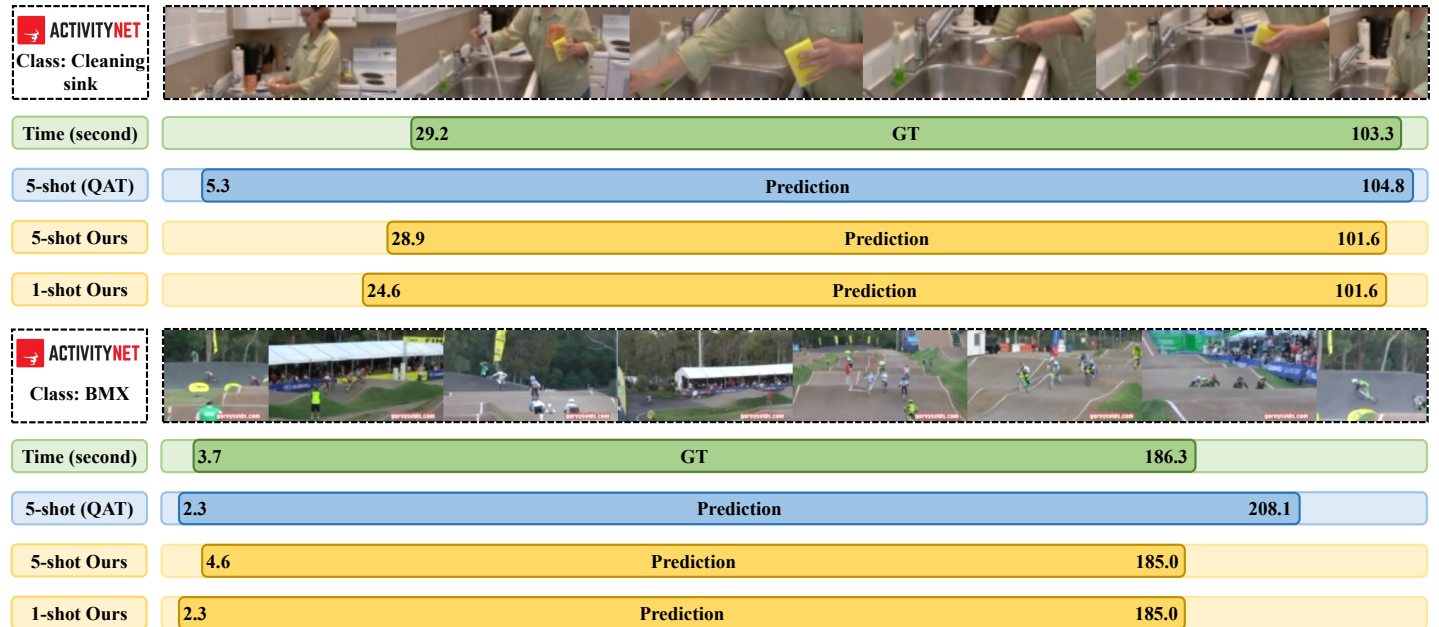


Fig. 8. Qualitative comparisons of our method (1-shot and 5-shot setting), QAT [5] (5-shot setting) and Ground Truth (GT) on “Cleaning sink” (single-instance) and “BMX” (single-instance) of ActivityNet1.3 dataset.

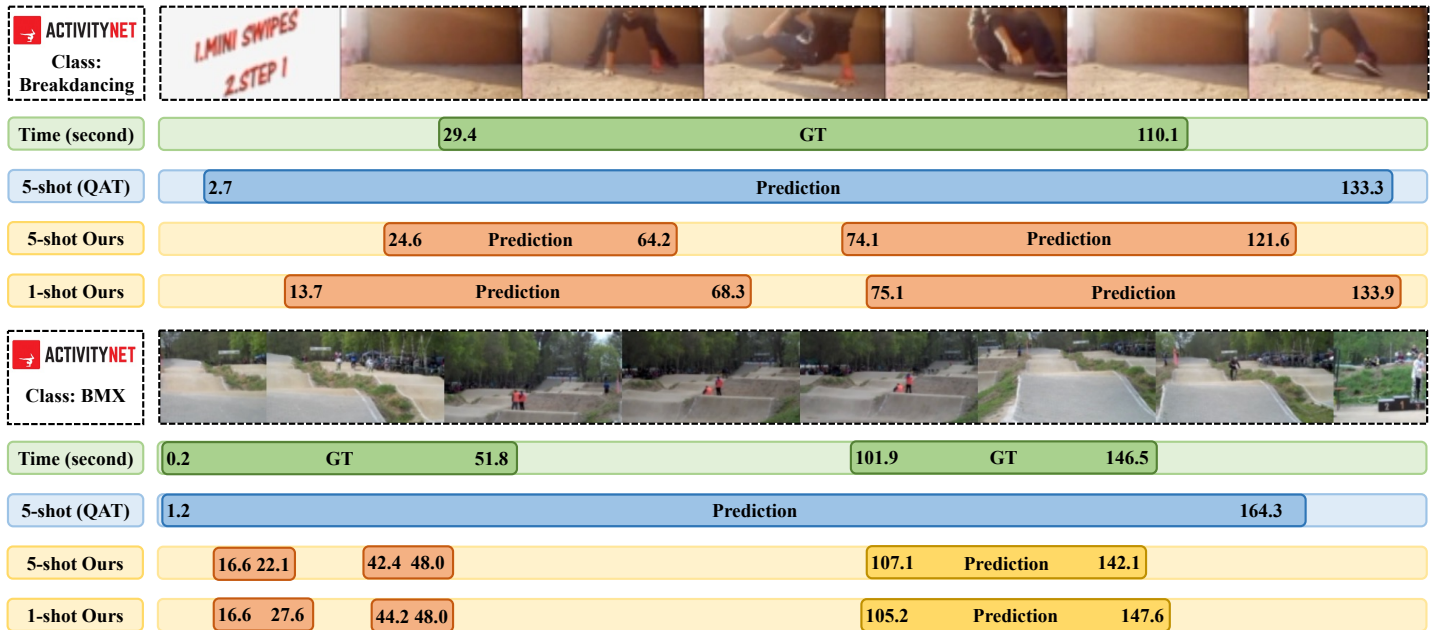


Fig. 9. Qualitative comparisons of our method (1-shot and 5-shot setting), QAT [5] (5-shot setting) and Ground Truth (GT) on “Breakdancing” (single-instance) and “BMX” (multi-instance) of ActivityNet1.3 dataset.

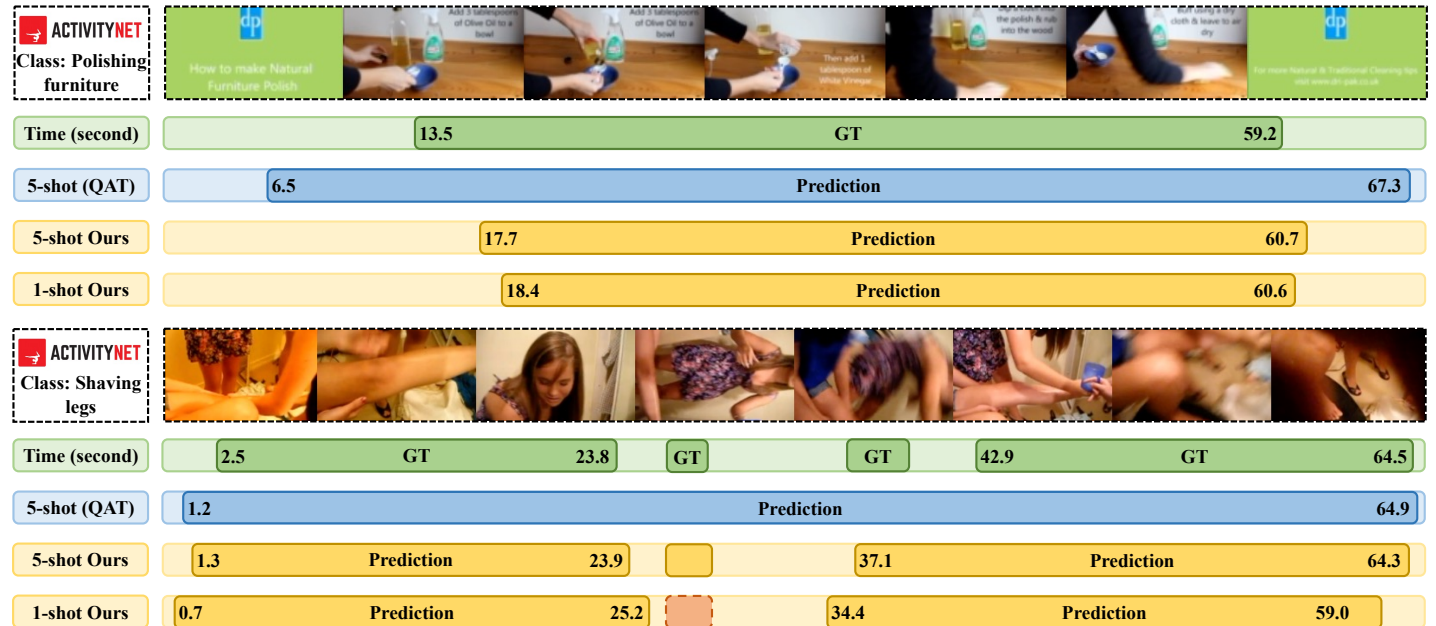


Fig. 10. Qualitative comparisons of our method (1-shot and 5-shot setting), QAT [5] (5-shot setting) and Ground Truth (GT) on “Rope skipping” (single-instance) and “Shaving legs” (multi-instance) of ActivityNet1.3 dataset.